NATIONAL ADVISORY COMMITTEE FOR AERONAUTICS

TECHNICAL NOTE 3744

SUPERSONIC FLOW PAST NONLIFTING BUMPED AND INDENTED BODIES OF REVOLUTION

By F. Edward McLean and Conrad Rennemann, Jr.

Langley Aeronautical Laboratory
Langley Field, Va.

NACA

Washington

September 1956

NATIONAL ADVISORY COMMITTEE FOR AERONAUTICS

TECHNICAL NOTE 3744

SUPERSONIC FLOW PAST NONLIFTING BUMPED AND INDENTED BODIES OF REVOLUTION

By F. Edward McLean and Conrad Rennemann, Jr.

SUMMARY

Linear theory is used to calculate the surface pressures, field pressures, and wave drag of nonlifting bumped and indented bodies of revolution in supersonic flow and the results are compared with the corresponding properties of a smooth basic body. The calculations show that relatively small surface irregularities cause large pressure disturbances both on the body and in the field. Application of a correction for the curvature of the characteristics substantially changes the nature of the pressure distribution, particularly in the disturbance field generated by a surface irregularity. The drag results indicate that, in general, the wave drag increases if volume is added to or subtracted from a smooth basic body so as to produce a surface irregularity on the basic body. The total wave drag of nonsmooth bodies consists of two relatively simple terms - the drag of the basic body and the drag of the body determined from the area distribution of the bump or indentation alone - and a complicated interference term. The interference parameters are presented for two body types and a range of values is suggested for use in obtaining a reasonable estimate of the wave drag of nonsmooth bodies.

INTRODUCTION

The aerodynamic characteristics of bodies of revolution at supersonic speeds have been considered in numerous investigations and several methods have been developed to describe the flow past such shapes. The method of characteristics and the linear theory approximations of Von Kármán (ref. 1), Lighthill (ref. 2), and Ward (ref. 3) have proven especially useful in this regard. Although many calculations have been made by using these methods, most have been limited to smooth bodies. With the advent of the area rule, however, there has been considerable interest in nonsmooth shapes.

The purpose of the present paper is to consider the aerodynamic properties of a simple class of nonsmooth bodies - namely, bodies of revolution which have irregularities in area distribution. Linear theory is used to calculate the surface pressures, field pressures, and wave

drag for nonlifting bumped and indented parabolic bodies of revolution in supersonic flow and the results are compared with the corresponding properties of a smooth basic body. The Whitham theory (ref. 4) is used to correct the field pressures for the curvature of the characteristics.

SYMBOLS

A cross-sectional area

B interference-drag parameter appearing in equation (14)

C_p pressure coefficient, $\frac{p - p_\infty}{q}$

D wave drag

$F(y) = \int_0^y \frac{f'(\xi)d\xi}{\sqrt{y - \xi}}$

f source-distribution function

$K = \frac{\gamma + 1}{\sqrt{2}} \frac{M^4}{\beta^{3/2}}$

l length of source distribution

M free-stream Mach number

N source-distribution constant

p local pressure

p_∞ free-stream pressure

q dynamic pressure, $\frac{1}{2} \rho U^2$

R body radius

U free-stream velocity

V volume

x,r axial and radial distances, respectively, in cylindrical coordinates

$\bar{x},\bar{r}$ coordinates defined by equations (12)

x_0 origin of bump or indentation source distribution

y characteristic number, $x - \beta r$

$\beta = \sqrt{M^2 - 1}$

Δ incremental value

γ ratio of specific heats

ξ dummy variable of integration

ρ free-stream density

ϕ disturbance velocity potential

Subscripts:

1 basic body

2 bump or indentation

SH Sears-Haack body

x partial derivative with respect to x

r partial derivative with respect to r

Primes denote derivatives with respect to the indicated argument of the function.

METHOD OF CALCULATION

The linearized differential equation for axisymmetric supersonic flow is

$$\beta^2\phi_{xx} - \phi_{rr} - \frac{1}{r}\phi_r = 0 \qquad (1)$$

where $\beta = \sqrt{M^2 - 1}$, M is the stream Mach number, and ϕ is the disturbance velocity potential. (The coordinate system is defined in fig. 1.) A solution of equation (1) for flow past a body of revolution can be expressed as

$$\phi = \frac{1}{2\pi}\int_0^{x-\beta r} \frac{f(\xi)d\xi}{\sqrt{(x - \xi)^2 - \beta^2 r^2}} \tag{2}$$

where $f(\xi)$ represents a distribution of sources along the axis of the body. The source distribution $f(\xi)$ is related to the body configuration by the boundary condition of zero normal velocity at the body surface. With the aid of mass-flow considerations (see ref. 5), this boundary condition can be written as

$$\pi R^2(x) = \int_0^{x-\beta R(x)} \frac{(x - \xi)f(\xi)d\xi}{\sqrt{(x - \xi)^2 - \beta^2 R^2(x)}} \tag{3}$$

where $R(x)$ is the body radius at any station x.

Inasmuch as the inverse of the integral equation (eq. 3) for the source strength is not known, the method of analysis adopted was to consider the source distribution as the primary variable. With this approach, nonsmooth bodies of revolution can be generated by the superposition of two known source distributions. The source distribution $f_1(x)$ gives rise to the basic body which lies between $x = 0$ and $x = l_1$. The bump or indentation is created by superposition of the source distribution $f_2(x)$ on $f_1(x)$ from $x = x_0$ to $x = x_0 + l_2$, where x_0 denotes the origin of f_2 and l_2 is the length of f_2. Thus,

$$\left.\begin{aligned} f(x) &= f_1(x) && \left(0 \leqq x \leqq x_0\right) \\ f(x) &= f_1(x) \pm f_2(x) && \left(x_0 \leqq x \leqq x_0 + l_2\right) \\ f(x) &= f_1(x) && \left(x_0 + l_2 \leqq x \leqq l_1\right) \end{aligned}\right\} \tag{4}$$

A plus sign before $f_2(x)$ corresponds to a bump and a minus sign, to an indentation.

The expressions for $f_1(x)$ and $f_2(x)$ used in the analysis are

$$\left.\begin{aligned} f_1(x) &= \frac{8\pi}{N_1^2 l_1^2}\left(l_1^2 x - 3l_1 x + 2x^3\right) \\ \text{and} \\ f_2(x) &= \frac{8\pi}{N_2^2 l_2^2}\left[l_2^2\left(x - x_0\right) - 3l_2\left(x - x_0\right)^2 + 2\left(x - x_0\right)^3\right] \end{aligned}\right\} \tag{5}$$

The functions $f_1(x)$ and $f_2(x)$ each give rise to a parabolic body of revolution in the slender-body approximation

$$f(x) = A'(x) \tag{6}$$

where $A(x)$ is the cross-sectional area distribution and the prime denotes the derivative with respect to the argument of the function. The parameter N_1 or N_2 which appears in equations (5) can be interpreted geometrically as the slender-body approximation (eq. 6) to the fineness ratio of the body generated by f_1 or f_2 alone.

Calculation of Body Shape

Equation (3) may be written in terms of the source distributions f_1 and f_2 as

$$\pi R^2(x) = \int_0^{x-\beta R(x)} \frac{(x - \xi) f_1(\xi)\, d\xi}{(x - \xi)^2 - \beta^2 R^2(x)} \pm \int_{x_0}^{x-\beta R(x)} \frac{(x - \xi) f_2(\xi)\, d\xi}{(x - \xi)^2 - \beta^2 R^2(x)} \tag{7}$$

The calculation of body shape from this equation is tedious inasmuch as $R(x)$ occurs in each term. Consequently, in the following paragraphs the equation is simplified and expressed in a form which partially separates the calculation of bump shape from the calculation of basic body shape.

For certain types of problems, it is well known that body shapes calculated by equation (3) can be closely approximated by preassigning a value to $R(x)$ on the right-hand side of the equation. If $R(x)/l$ is small compared with unity, $R(x)$ may be set equal to zero and the equation reduces to the simple slender-body relation (eq. 6). For quasi-cylindrical configurations (ref. 2), $R(x)$ may be assigned a constant value on the right-hand side of equation (3). In reference 6, which considers the problem of boattail bodies of revolution having minimum drag, $R(x)$ is assigned the values corresponding to the cone that passes through the nose and base of the body.

The approximate methods outlined suggest that some reasonable simplifications can be made in equation (7). For the body shapes considered herein, $R(x)$ is very small compared with the length of f_1 and, consequently, the slender-body approximation can be made in the first integral of equation (7). However, inasmuch as $R(x)$ is not necessarily small compared with the length of f_2, some other approximation is required in the second integral. An approximation that has the merit of simplicity and accuracy is to replace $R(x)$ in the second integral of equation (7) with the radius of the basic body as determined from the slender-body relation $2\pi R_1(x)R_1'(x) = f_1(x)$. Then

$$\pi R^2(x) = \int_0^x f_1(\xi)d\xi \pm \int_{x_0}^{x-\beta R_1(x)} \frac{(x - \xi)f_2(\xi)d\xi}{\sqrt{(x - \xi)^2 - \beta^2 R_1^2(x)}} \tag{8}$$

where the first integral represents the area distribution of the slender basic body and the second integral, which for a given Mach number depends only on $R_1(x)$ and f_2, represents the area distribution of the surface irregularity.

A comparison of the bump area distributions ΔA as obtained from equations (6), (7), and (8) for $N_1 = 12$, $N_2 = 8$, $x_0/l_1 = 0.50$, $l_2/l_1 = 0.25$, and $M = \sqrt{2}$ is presented in figure 2 and a comparison of the total area distribution is shown in figure 3. The approximation afforded by equation (8) for both the bump area and the total area is considered satisfactory, whereas the slender-body approximation (eq. 6) is considered inadequate for the calculation of nonsmooth shapes.

Calculation of Pressure Field

Linear theory.- The linearized pressure coefficient at any point in the field is given by

$$C_p = -2\phi_x - \phi_r^2 \tag{9}$$

where

$$\phi_x = -\frac{1}{2\pi}\int_0^{x-\beta r} \frac{f'(\xi)d\xi}{\sqrt{(x-\xi)^2 - \beta^2 r^2}} \tag{10}$$

and

$$\phi_r = \frac{1}{2\pi r}\int_0^{x-\beta r} \frac{(x-\xi)f'(\xi)d\xi}{\sqrt{(x-\xi)^2 - \beta^2 r^2}} \tag{11}$$

Whitham's correction.- It is well known that linear theory does not provide a first-order approximation to the flow field at supersonic speeds and that the approximation becomes worse as the distance from the body is increased. This fact led Whitham (ref. 4) to develop a method for correcting the linear flow fields so that a first approximation is obtained everywhere. Whitham's basic hypothesis is that linear theory gives the correct values for the velocity components but locates them incorrectly. By taking the curvature of the characteristics into account, Whitham deduces that the values of $\phi_x(x,r)$ and $\phi_r(x,r)$ should be located at the coordinates $(\bar{x},\bar{r})$ where

$$\left.\begin{aligned} \bar{r} &= r \\ \bar{x} &= \beta r - KF(y)\sqrt{r} + y \end{aligned}\right\} \tag{12}$$

In equation (12)

$$y = x - \beta r$$

$$F(y) = \int_0^y \frac{f'(\xi)d\xi}{\sqrt{y-\xi}}$$

and

$$K = \frac{\gamma + 1}{\sqrt{2}} \frac{M^4}{\beta^{3/2}}$$

When the flow-field data are relocated by means of equation (12), it is found that, in some cases, the characteristic lines cross. Whitham interprets such intersections as indications of the presence of shock waves. Reference 4 presents further details and an interesting graphical method of locating the shock waves from the $F(y)$ curve.

Calculation of Wave Drag

The wave drag of a distribution of sources along an axis can be related to the momentum transfer through a cylindrical surface enclosing the axis. The expression for the wave drag is then obtained (see ref. 1, for example) as

$$\frac{2\pi D}{q} = -\int_0^{l_1}\int_0^{l_1} f'(x)f'(\xi)\log_e|x - \xi|\,dx\,d\xi \tag{13}$$

where D is the wave drag and q is the dynamic pressure. When the source distributions given by equation (4) are substituted into equation (13) and the indicated integrations performed, the wave drag can be written as

$$\frac{D}{D_1} = 1 \pm B\left(\frac{N_1}{N_2}\right)^2\left(\frac{l_2}{l_1}\right) + \frac{D_2}{D_1}$$

or

$$\frac{D}{D_1} = 1 \pm B\left(\frac{N_1}{N_2}\right)^2\left(\frac{l_2}{l_1}\right) + \left(\frac{N_1}{N_2}\right)^4\left(\frac{l_2}{l_1}\right)^2 \tag{14}$$

where D_1 is the wave drag of the basic source distribution f_1 alone, D_2 is the wave drag of f_2 alone, and D is the total wave drag which results from the combination of f_1 and f_2. A plus sign preceding the second term on the right-hand side of equation (14) corresponds to a bump on the basic body and a minus sign corresponds to an indentation. The factor B appearing in the equation is a complicated function of x_0/l_1 and l_2/l_1.

RESULTS AND DISCUSSION

Body Shape

Scale drawings of the basic, bumped, and indented bodies considered herein are presented in figure 4. These shapes were calculated from the basic mass-flow boundary condition (eq. (7)) for $N_1 = 12$, $N_2 = 8$, $x_0/l_1 = 0.50$, $l_2/l_1 = 0.25$, and $M = \sqrt{2}$. The differences between the basic body shape and the shapes of the bumped and indented bodies appear small for the case selected. In order to illustrate more clearly the magnitude of the area change introduced by the surface irregularities, the cross-sectional area distributions of these bodies are presented in figure 5.

The variation of bump area distribution with the strength of the bump source distribution is shown in figure 6, where bump area distributions are presented for values of $N_2 = 6$, 8, and 10. The indentations for corresponding values of N_2 are slightly different from the bump area distributions shown inasmuch as body shapes calculated from equation (7) are influenced by the differences between the radii of the bumped and indented bodies. If equation (8) is used to calculate body shape, however, the area distributions of corresponding bumps and indentations are the same.

Pressure Field

The surface pressure distributions for the basic, bumped, and indented bodies corresponding to values of $N_1 = 12$, $x_0/l_1 = 0.50$, $l_2/l_1 = 0.25$, $M = \sqrt{2}$, and $N_2 = 6$, 8, and 10 are presented in figure 7. Although the surface irregularities considered make only small visual changes in body shape (for example, see fig. 4), the surface pressure disturbances caused by the irregularities are seen to be relatively large. It should be pointed out, however, that viscous effects would probably reduce the magnitudes of the pressure disturbances arising from such small surface irregularities.

In the limit as the bump length goes to zero, the change in surface pressure coefficient due to the bump can be obtained exactly from the two-dimensional pressure relation $\Delta C_p = \frac{2}{\beta} \Delta R'$, where $\Delta R'$ is the change

in body slope due to f_2. A comparison of the values of ΔC_p at the surface as obtained from equation (9) and the two-dimensional relation is presented in figure 8 for the bump considered in the present paper.

Field-pressure coefficients, with and without the Whitham correction, for the basic, bumped, and indented bodies (fig. 4), are presented in figures 9, 10, and 11, respectively. Pressure distributions for each body shape are given at the four field locations $r/l_1 = 0.125$, 0.250, 0.500, and 1.0.

The shift of the field pressures predicted by the Whitham theory for the basic body (fig. 9), although significant, is not large at the field locations shown, and the predicted shock at the nose of the body affects only a small portion of the field. However, the Whitham correction in the region of the bump or indentation (figs. 10 and 11) is relatively large at all field stations represented, and the predicted shocks have a marked effect on the pressure distribution.

In order to illustrate the nature of the calculated flow field about the basic, bumped, and indented bodies, sketches of the Whitham corrected characteristics and shock locations are presented in figure 12. In the region of the surface irregularity the corrected characteristics exhibit considerable curvature, whereas the linear characteristics would have no curvature and would point downstream at an angle of 45° from the body center line.

Wave Drag

The variation of D/D_1 with N_1/N_2 as calculated from equation (14) for both bumped and indented bodies is presented in figure 13 for $l_2/l_1 = 0.25$ with $x_0/l_1 = 0$ and 0.375, and for $l_2/l_1 = 0.50$ with $x_0/l_1 = 0$ and 0.25. The values of x_0/l_1 chosen bracket the range of D/D_1 for the given l_2/l_1; that is, the value of D/D_1 for other values of x_0/l_1 and the given l_2/l_1 lie between the curves shown. Some of the curves correspond to two locations of the source distribution f_2: For example, the bumped-body curve for $l_2/l_1 = 0.25$ and $x_0/l_1 = 0.75$ is identical to that for $x_0/l_1 = 0$. It should be noted, however, that the drag of a given nonsmooth body is not exactly the same in a forward and reverse flow because the bump area depends upon both the bump source strength and the configuration of the basic body. (See eq. (8).)

Examination of figure 13 shows that in most cases the wave drag increases if volume is either added to or subtracted from a smooth basic

body so as to produce a surface irregularity on the basic body. For example, the bumped and indented bodies (fig. 4) have 41 percent and 22 percent more drag, respectively, than the smooth basic body.

According to figure 13, the ratios l_2/l_1 and N_1/N_2 are of primary importance in the determination of the drag, whereas the location of the surface irregularity is of secondary importance. The latter conclusion might have been anticipated from a result of Robert T. Jones presented in reference 7 that, for a Sears-Haack basic body, the drag increment due to adding or subtracting a bump is independent of the location of the bump. If f_{SH} denotes the source distribution which would give rise to a Sears-Haack body in the slender-body approximation and f_2 denotes any other source distribution shorter than f_{SH}, Jones found that the drag of the shape given by superposition of f_2 on f_{SH} can be expressed as

$$\frac{D}{D_{SH}} = 1 + 2\frac{V_2}{V_{SH}} + \frac{D_2}{D_{SH}} \tag{15}$$

In equation (15), D_2 denotes the drag of f_2 alone and D_{SH} denotes the drag of f_{SH} alone. The symbols V_2 and V_{SH} are to be interpreted in a manner similar to that for N for the parabolic shapes; that is, V_2 $\left(\text{or } V_{SH}\right)$ is the volume of the body defined by equation (6) for f_2 $\left(\text{or } f_{SH}\right)$ alone.

The expressions for the drag given by equations (14) and (15) naturally separate into three parts - the drag of the basic body alone, the drag of a body determined by the volume of the bump or indentation alone, and an interference drag. In general, the drag of the separate components can be calculated quite easily, whereas the computation of the interference drag is rather involved. It is noteworthy that Jones discovered a case for which the interference drag is given by such a simple expression.

When equation (15) is written in the form of equation (14) for two Sears-Haack source distributions, the interference-drag parameter B is given by

$$B = 2\left(\frac{l_2}{l_1}\right)^2_{SH}$$

These values of B are shown in figure 14 for comparison with those appearing in equation (14) for the parabolic shapes considered in this paper. There is general agreement between the magnitudes of B for the various length ratios. This agreement suggests the possibility of obtaining a rapid estimate of the drag of nonsmooth shapes by selection of a value of B from figure 14 on the basis of length ratio alone.

CONCLUDING REMARKS

The supersonic pressure field and wave drag of nonlifting bumped and indented bodies of revolution are calculated by linear theory and the results are compared with the corresponding properties of a smooth body. A comparison of the calculated pressure distributions indicates that relatively small surface irregularities cause large pressure disturbances both on the body and in the field. Application of a correction for the curvature of the characteristics substantially changes the nature of the pressure distribution, particularly in the disturbance field generated by a surface irregularity. The drag results indicate that, in general, the wave drag increases if volume is added to or subtracted from a smooth basic body so as to produce a surface irregularity on the basic body. The total wave drag of nonsmooth bodies consists of two relatively simple terms - the drag of the basic body and the drag of the body determined from the cross-sectional area distribution of the bump or indentation alone - and a complicated interference term. The interference parameters are presented for two body types and a range of values is suggested for use in obtaining a reasonable estimate of the drag of nonsmooth bodies.

Langley Aeronautical Laboratory,
National Advisory Committee for Aeronautics,
Langley Field, Va., May 14, 1956.

REFERENCES

1. Von Kármán, Th.: The Problem of Resistance in Compressible Fluids. R. Accad. d'Italia, Cl. Sci. Fis., Mat. e Nat., vol. XIV, 1936. (Fifth Volta Congress held in Rome, Sept. 30 - Oct. 6, 1935.)

2. Lighthill, M. J.: Supersonic Flow Past Bodies of Revolution. R. & M. No. 2003, British A.R.C., 1945.

3. Ward, G. N.: Supersonic Flow Past Slender Pointed Bodies. Quarterly Jour. Mech. and Appl. Math., vol. II, pt. 1, Mar. 1949, pp. 75-97.

4. Whitham, G. B.: The Flow Pattern of a Supersonic Projectile. Communications on Pure and Appl. Math., vol. V, no. 3, Aug. 1952, pp. 301-348.

5. Parker, Hermon M.: Minimum-Drag Ducted and Pointed Bodies of Revolution Based on Linearized Supersonic Theory. NACA Rep. 1213, 1955. (Supersedes NACA TN 3189.)

6. Harder, Keith C., and Rennemann, Conrad, Jr.: On Boattail Bodies of Revolution Having Minimum Wave Drag. NACA TN 3478, 1955.

7. Lomax, Harvard, and Heaslet, Max. A.: A Special Method for Finding Body Distortions That Reduce the Wave Drag of Wing and Body Combinations at Supersonic Speeds. NACA RM A55B16, 1955.

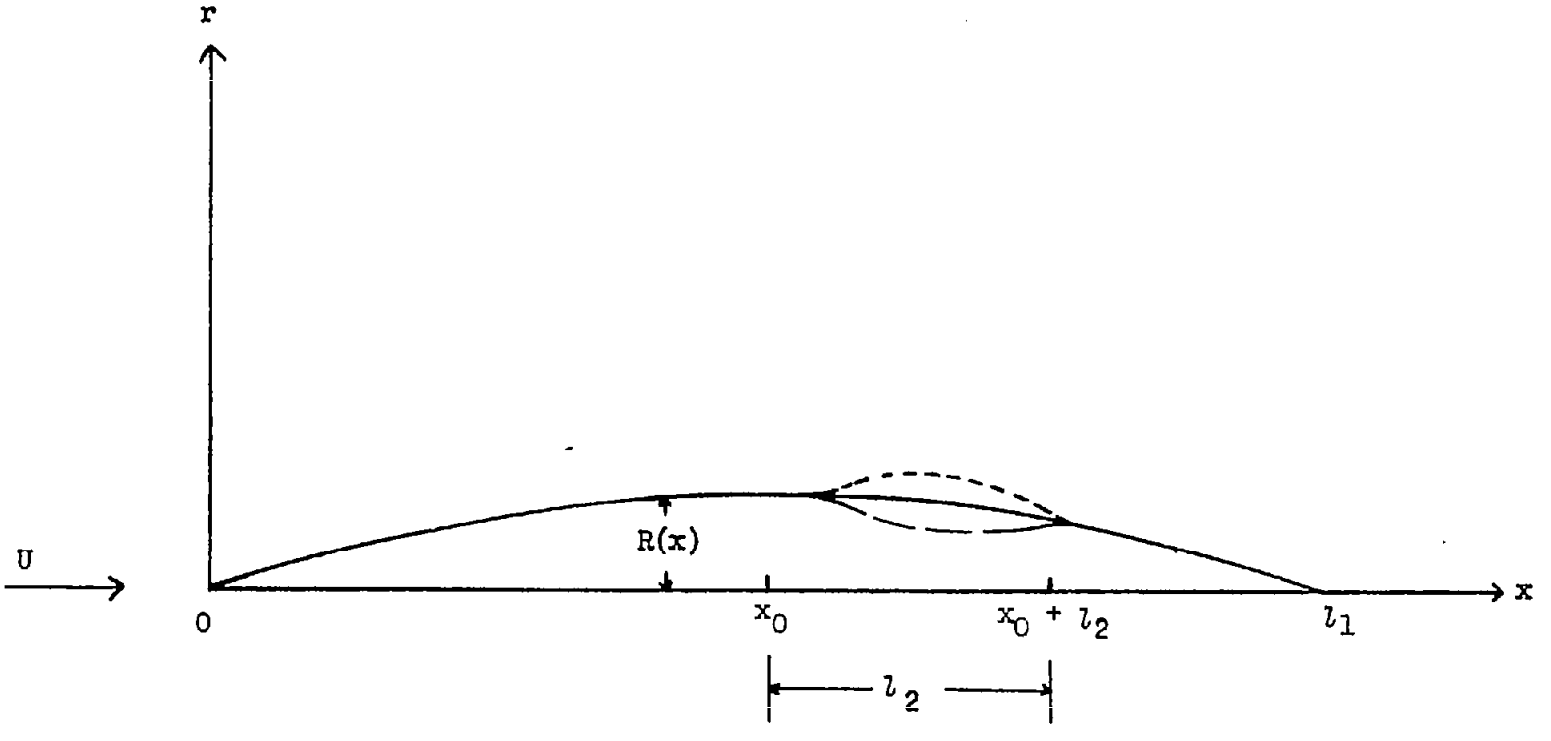

Figure 1.- Coordinate system.

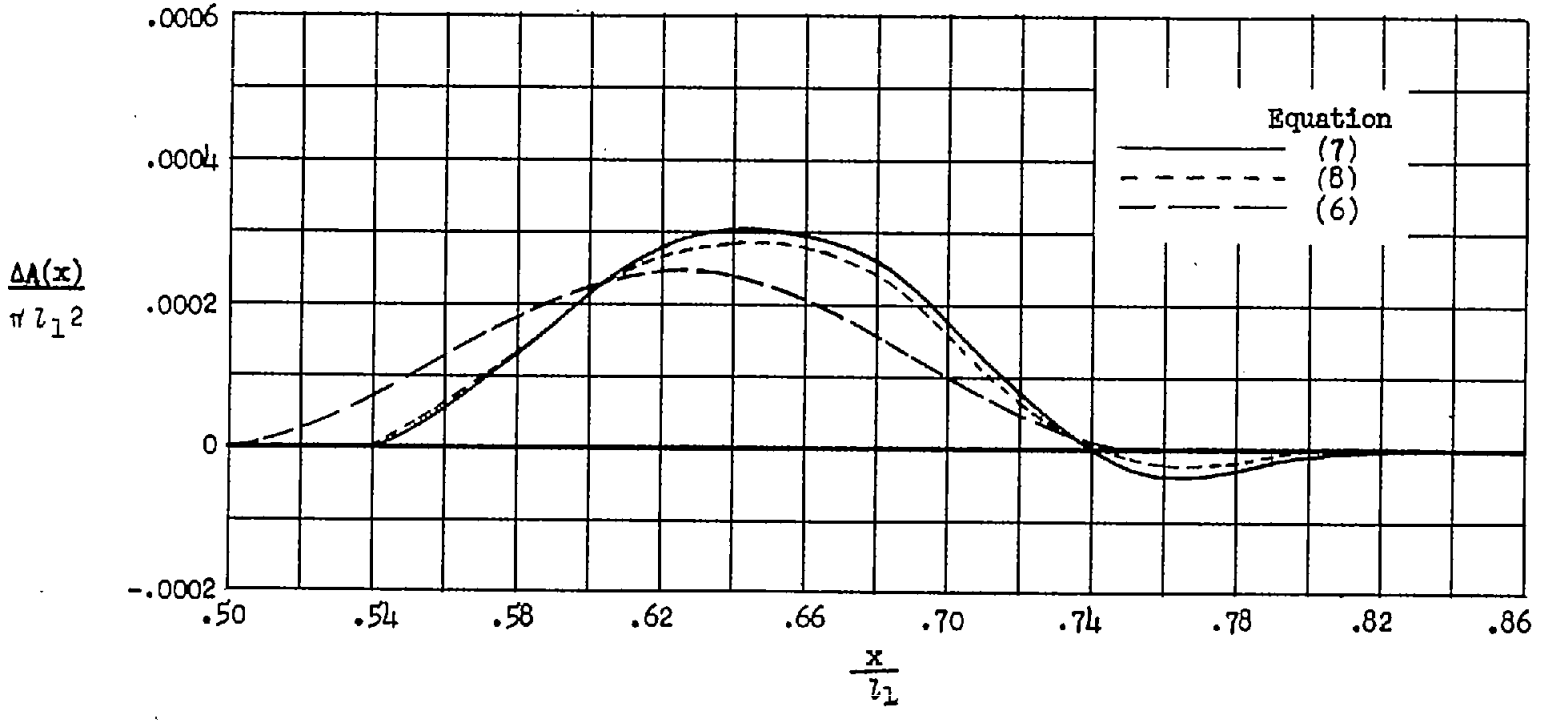

Figure 2.- Comparison of changes in body area introduced by a bump source distribution as calculated from equations (6), (7), and (8). $N_1 = 12$; $N_2 = 8$; $\frac{x_0}{l_1} = 0.50$; $\frac{l_2}{l_1} = 0.25$; $M = \sqrt{2}$.

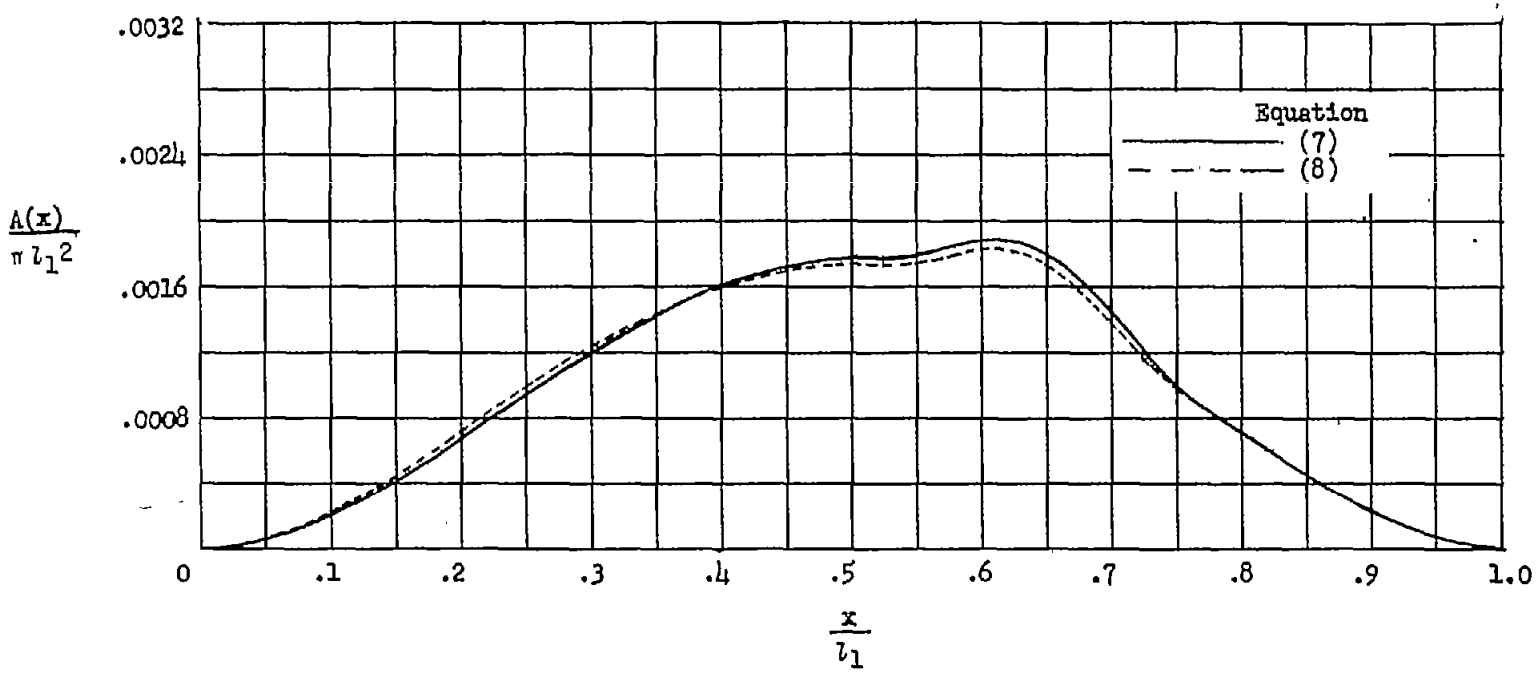

Figure 3.- Comparison of the total area distributions of a bumped body as calculated from equations (7) and (8). $N_1 = 12$; $N_2 = 8$; $\frac{x_0}{l_1} = 0.50$; $\frac{l_2}{l_1} = 0.25$; $M = \sqrt{2}$.

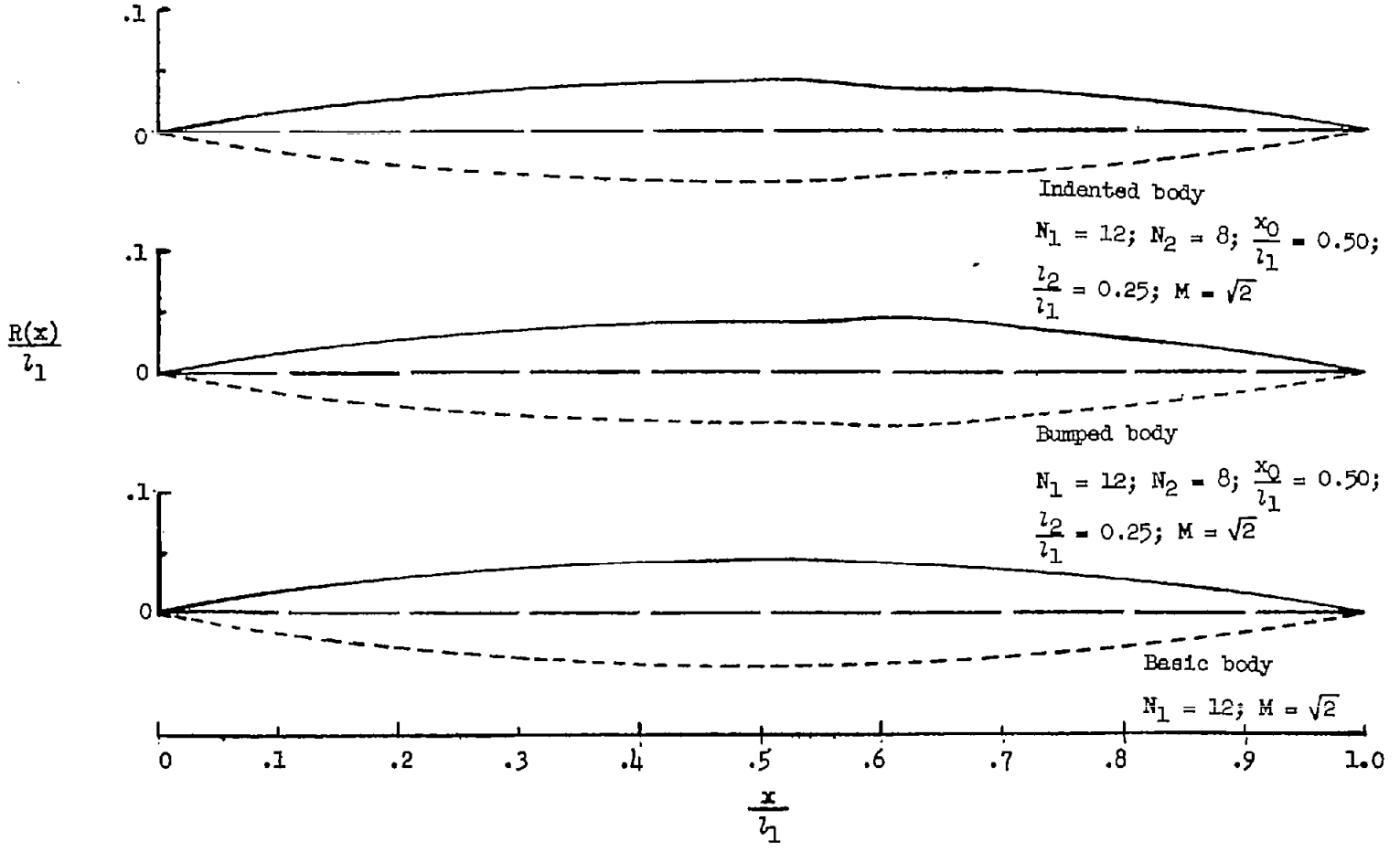

Figure 4.- Scale drawings of the basic, bumped, and indented bodies selected for the study of field pressure distribution.

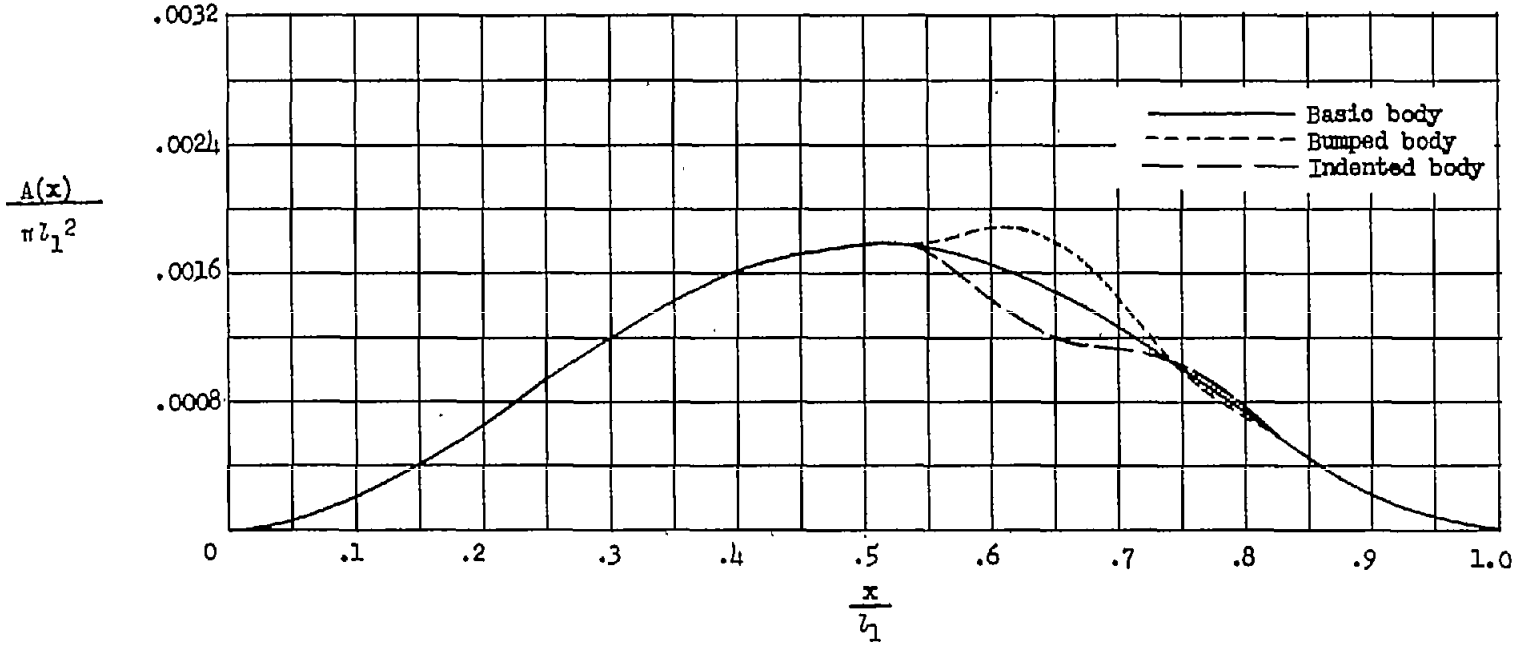

Figure 5.- Cross-sectional area distributions of the basic, bumped, and indented bodies of figure 4.

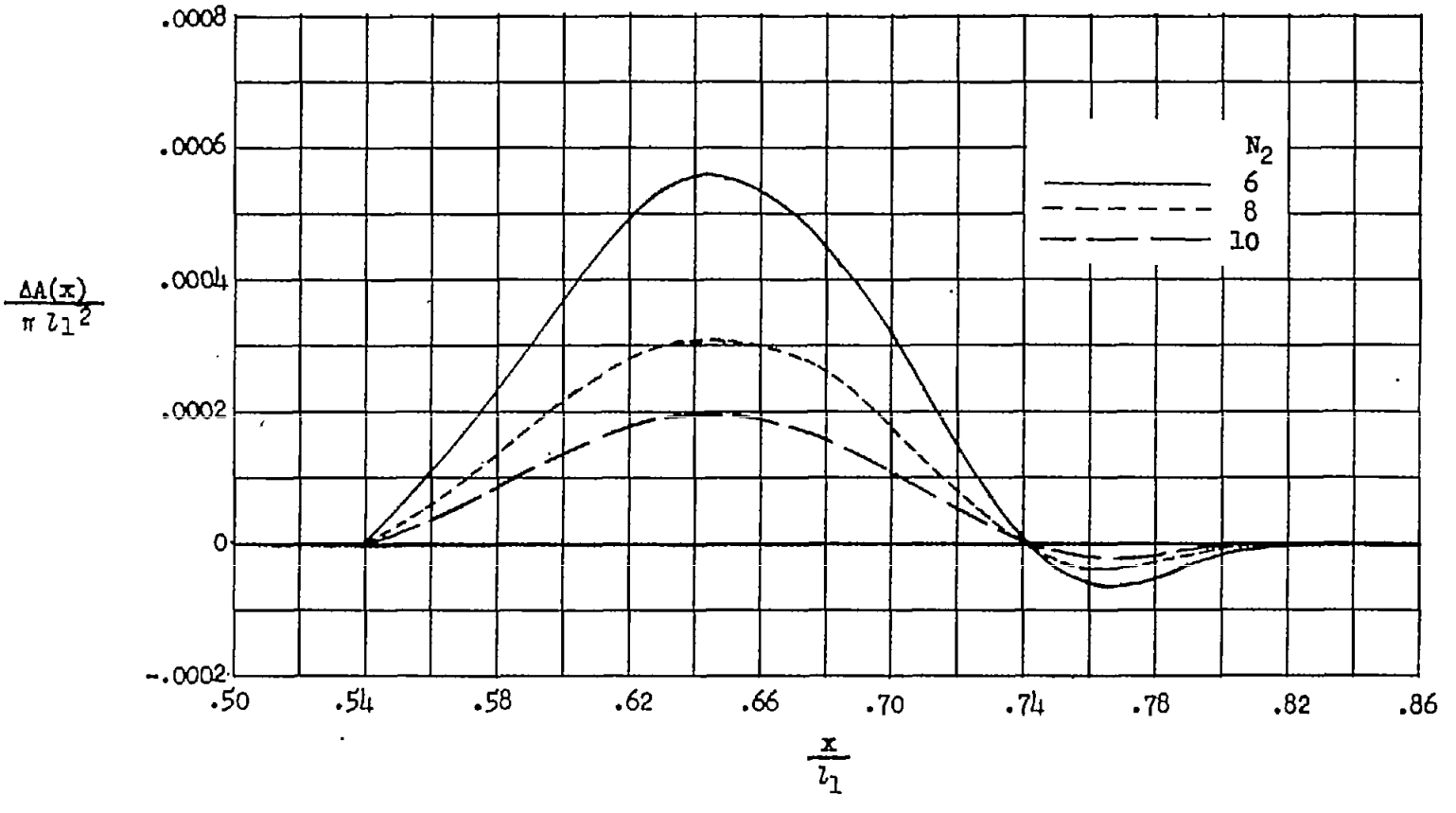

Figure 6.- Effect of N_2 on changes in body area introduced by a bump source distribution. $N_1 = 12$; $\frac{x_0}{l_1} = 0.50$; $\frac{l_2}{l_1} = 0.25$; $M = \sqrt{2}$.

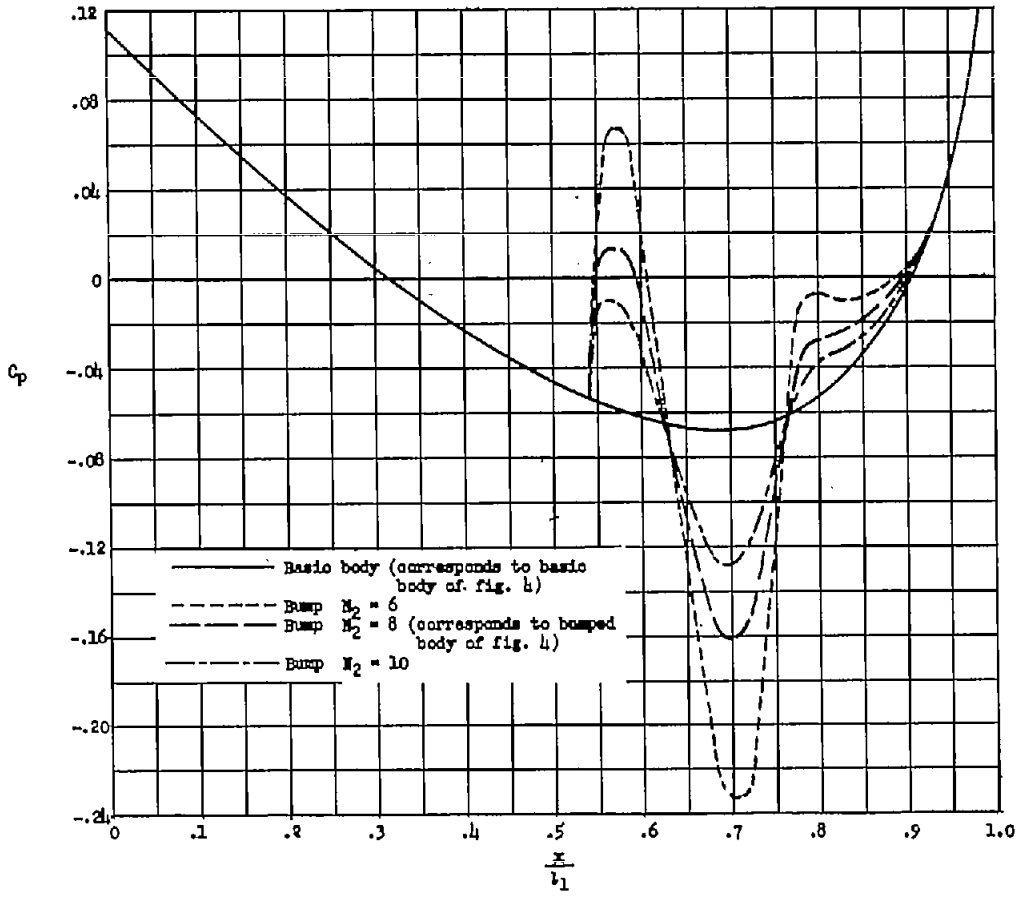

(a) Basic and bumped bodies.

Figure 7.- Surface pressure distributions for basic, bumped, and indented bodies. $N_1 = 12$; $\frac{x_0}{l_1} = 0.50$; $\frac{l_2}{l_1} = 0.25$; $M = \sqrt{2}$.

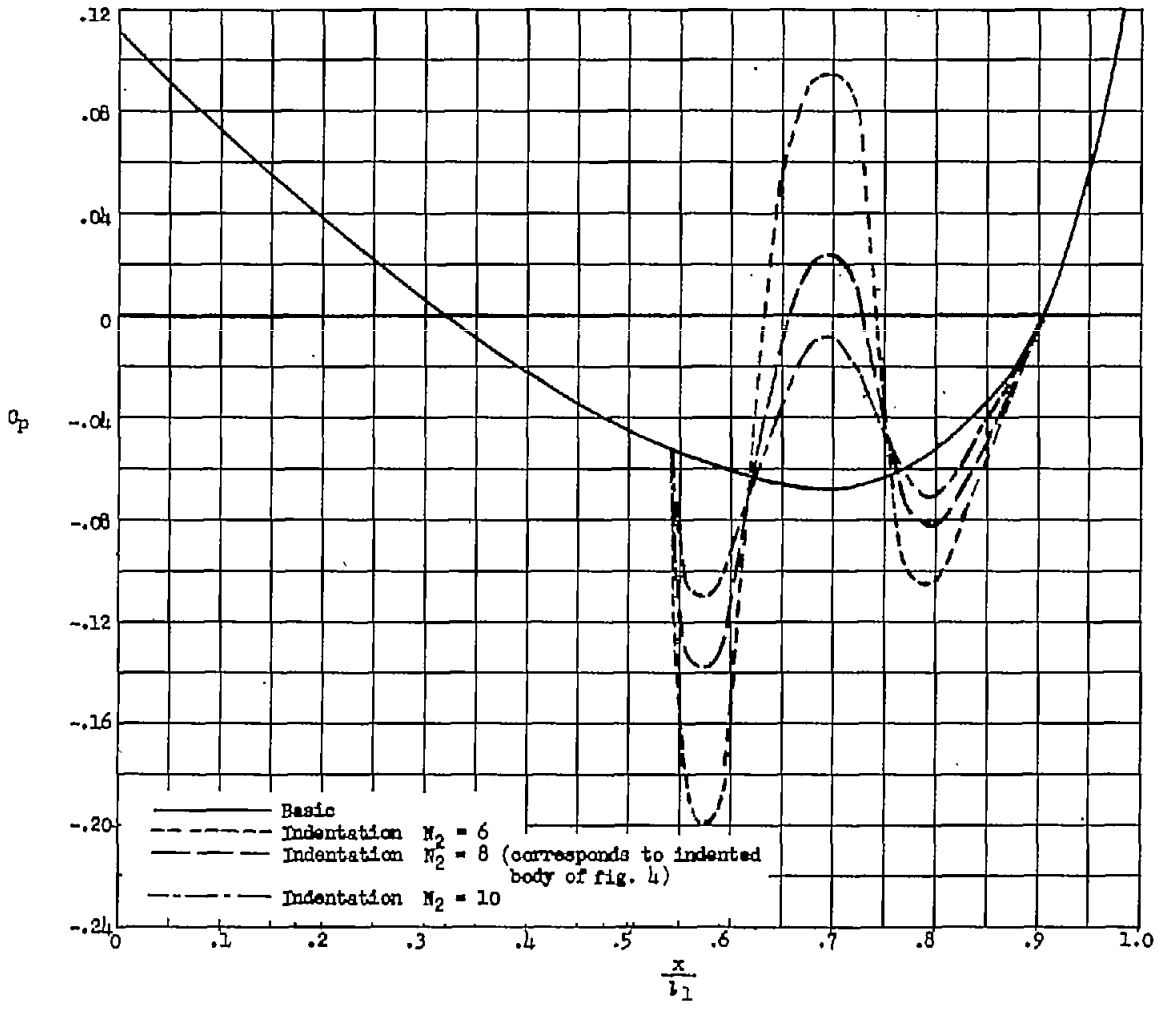

(b) Basic and indented bodies.

Figure 7.- Concluded.

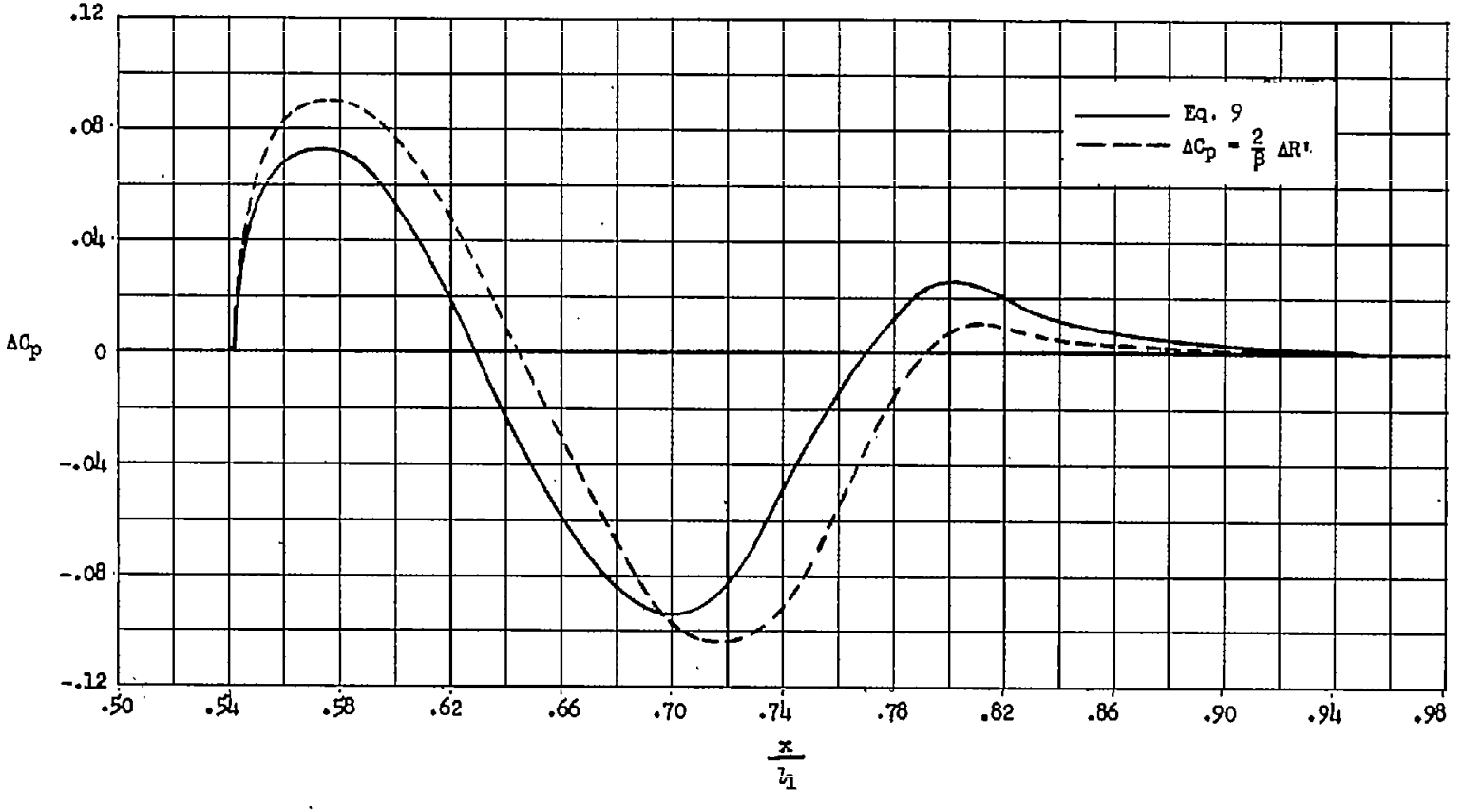

Figure 8.- Comparison of the change in surface pressure coefficient due to a bump as calculated from equation (9) and from the two-dimensional pressure relation $\Delta C_p = \frac{2}{\beta} \Delta R'$. $N_1 = 12$; $N_2 = 8$; $\frac{x_0}{l_1} = 0.50$; $\frac{l_2}{l_1} = 0.25$; $M = \sqrt{2}$.

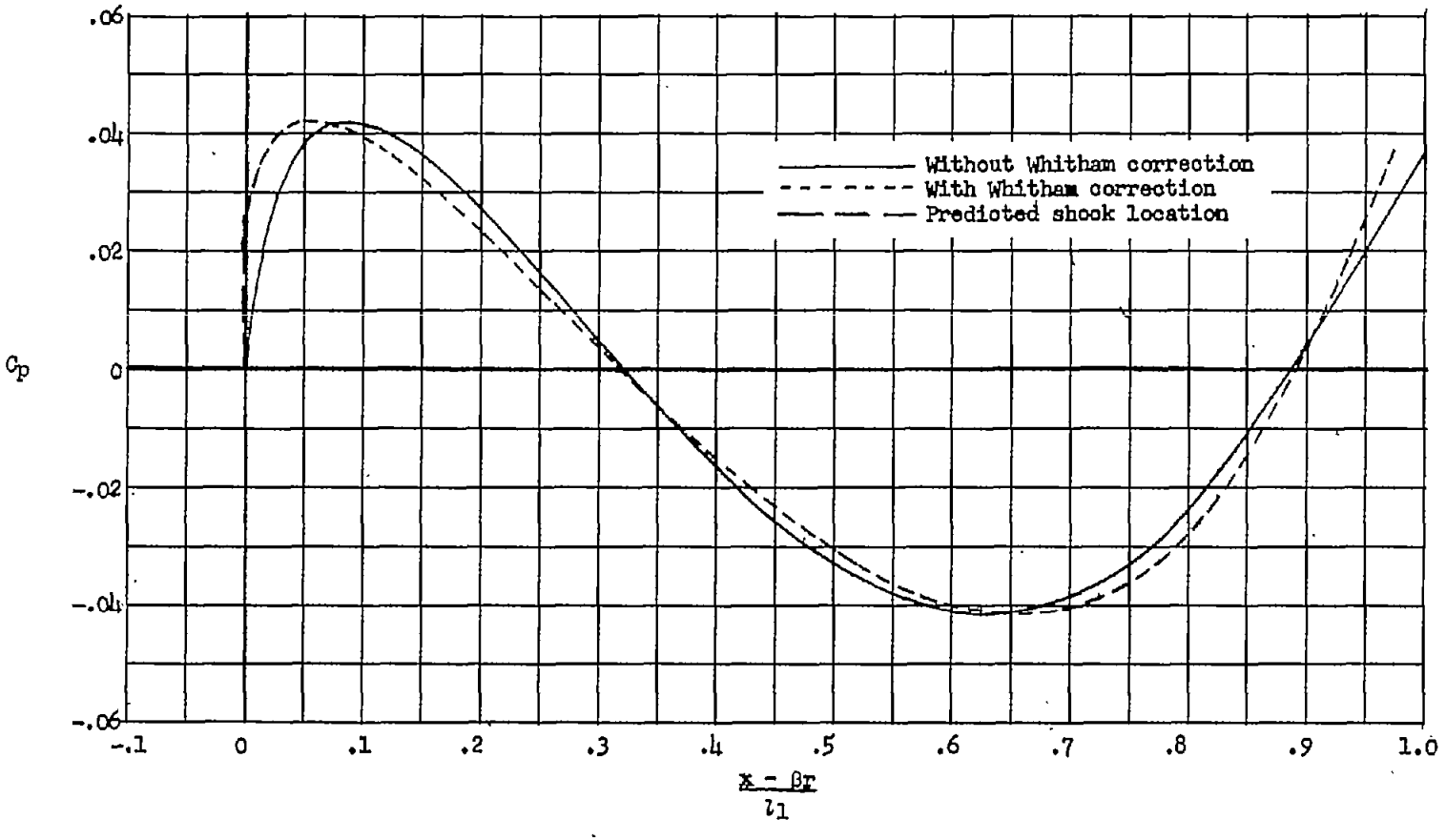

(a) $\frac{r}{l_1} = 0.125$.

Figure 9.- Linear field pressure distributions, with and without Whitham correction, for basic body of figure 4. $M = \sqrt{2}$.

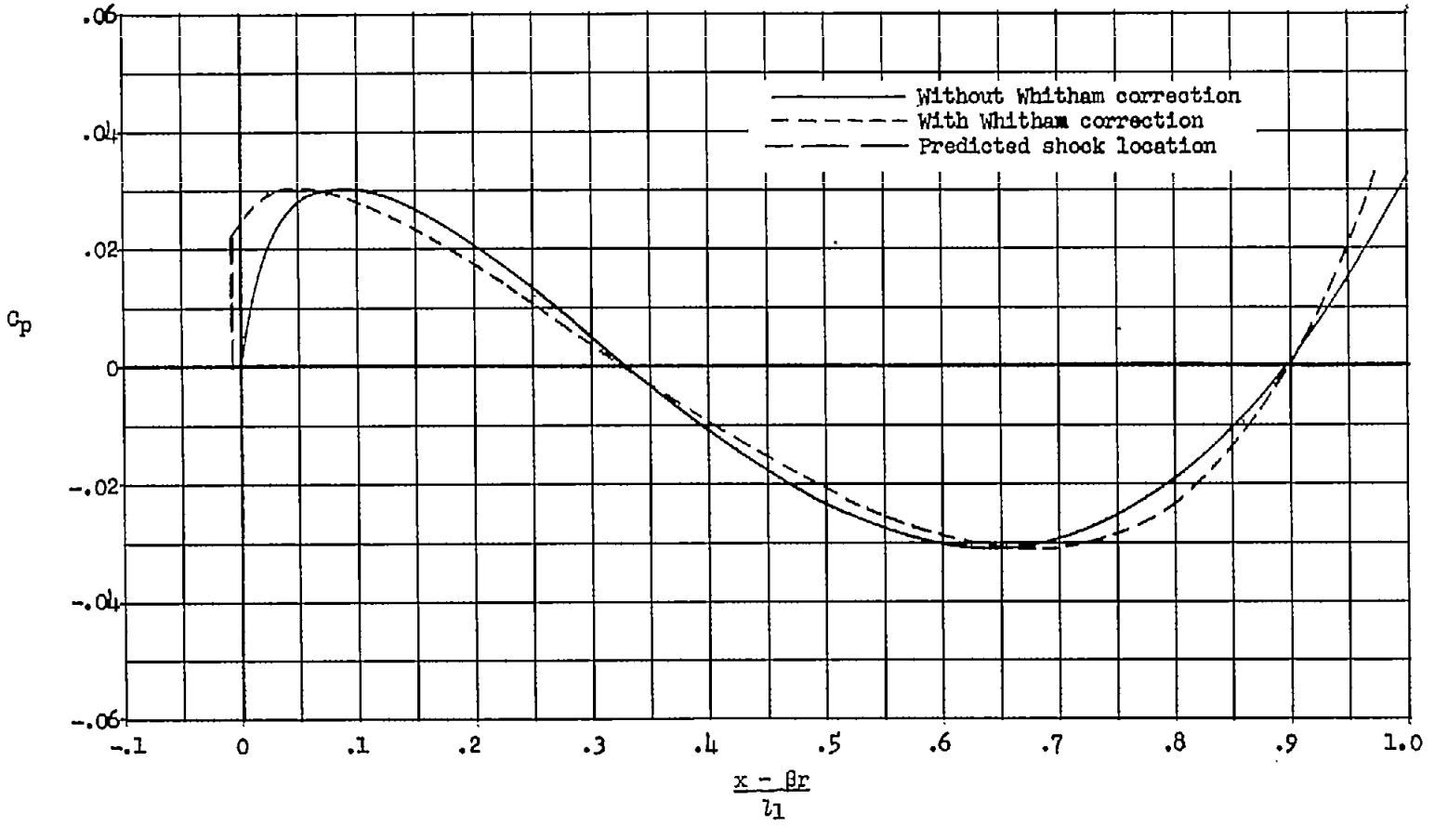

(b) $\frac{r}{l_1} = 0.250$.

Figure 9.- Continued.

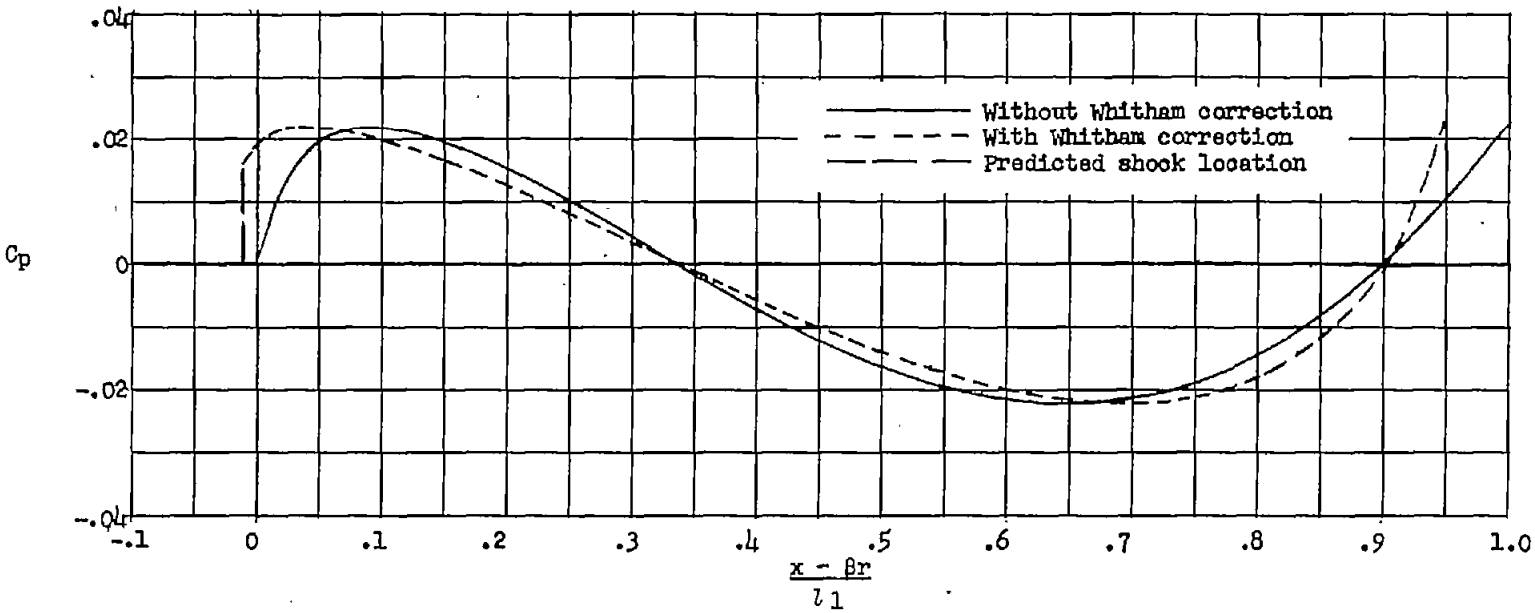

(c) $\frac{r}{l_1} = 0.500.$

Figure 9.- Continued.

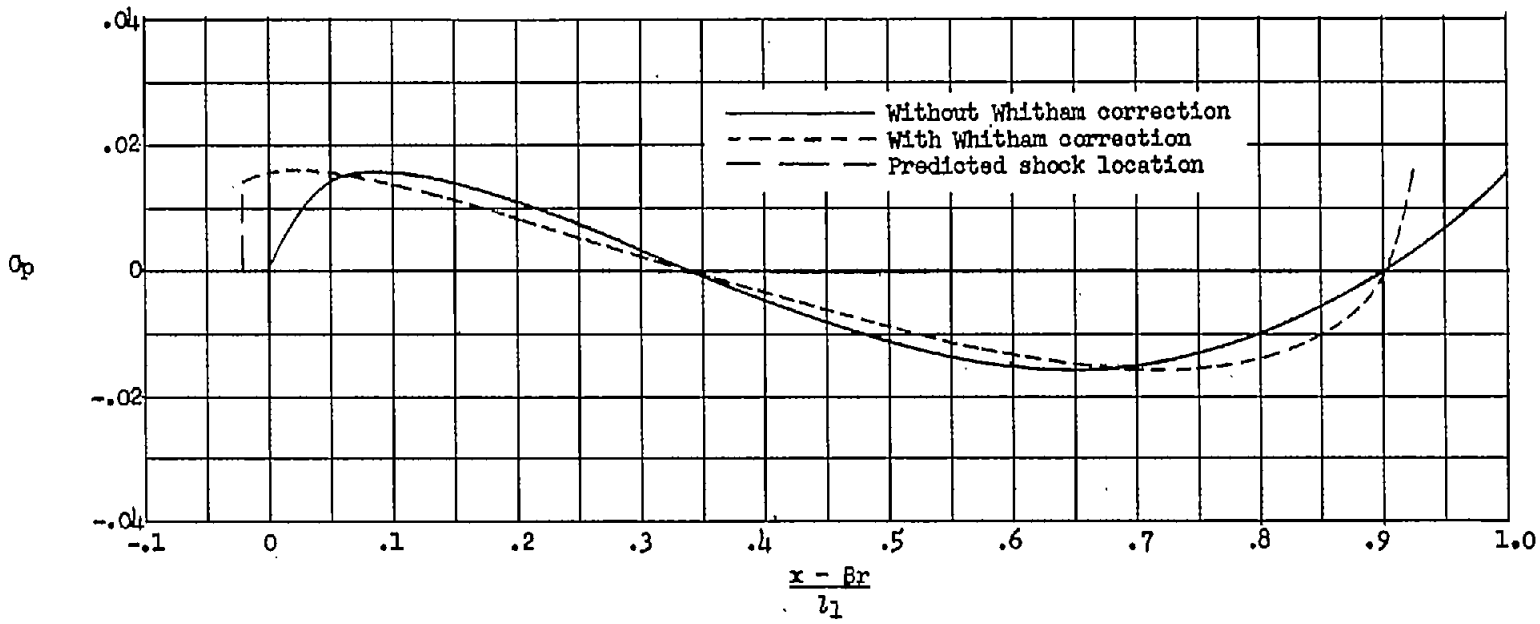

(d) $\frac{r}{l_1} = 1.0$.

Figure 9.- Concluded.

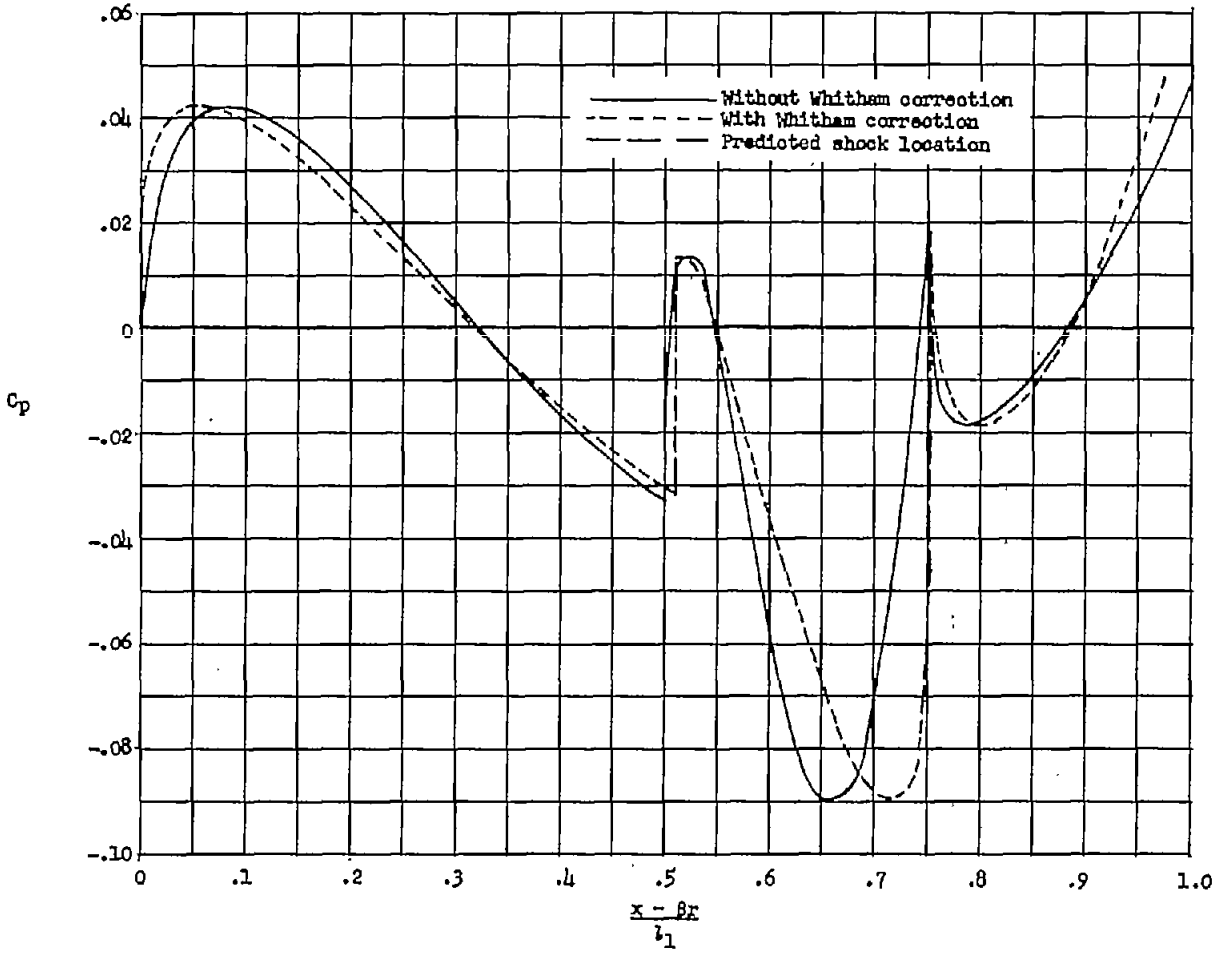

(a) $\frac{r}{l_1} = 0.125$.

Figure 10.- Linear field pressure distributions, with and without Whitham correction, for bumped body of figure 4. $M = \sqrt{2}$.

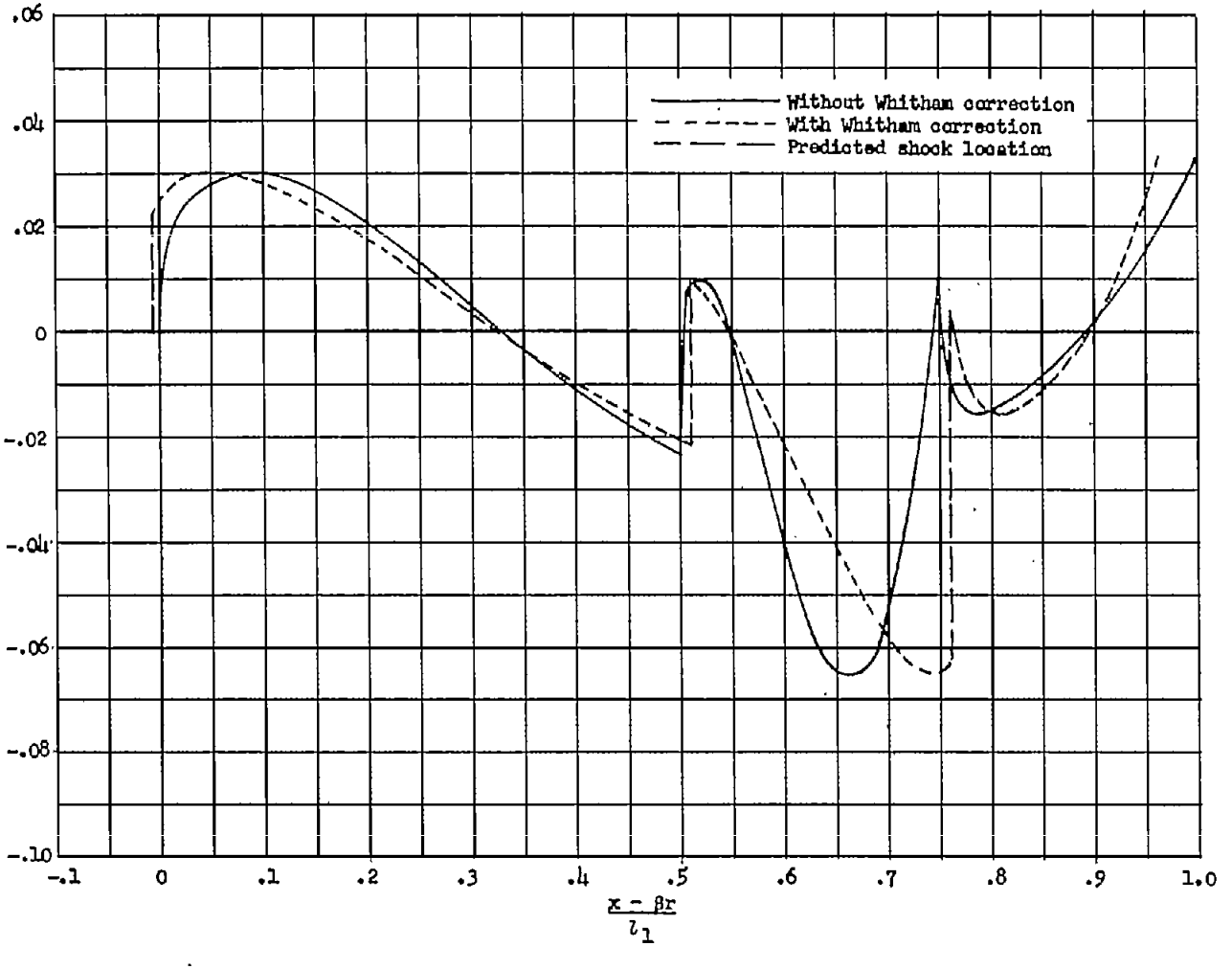

(b) $\frac{r}{l_1} = 0.250$.

Figure 10.- Continued.

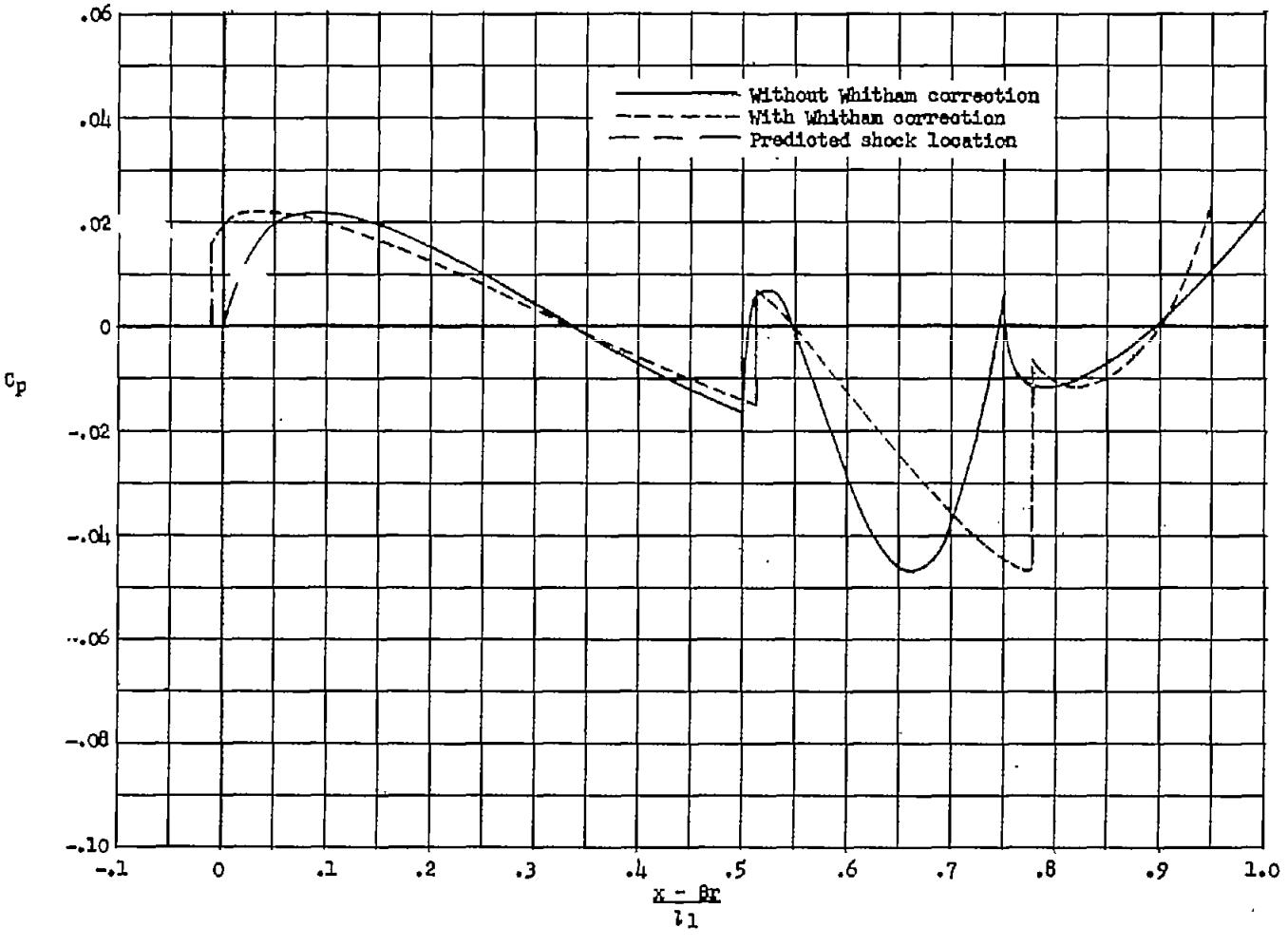

(c) $\frac{r}{l_1} = 0.500$.

Figure 10.- Continued.

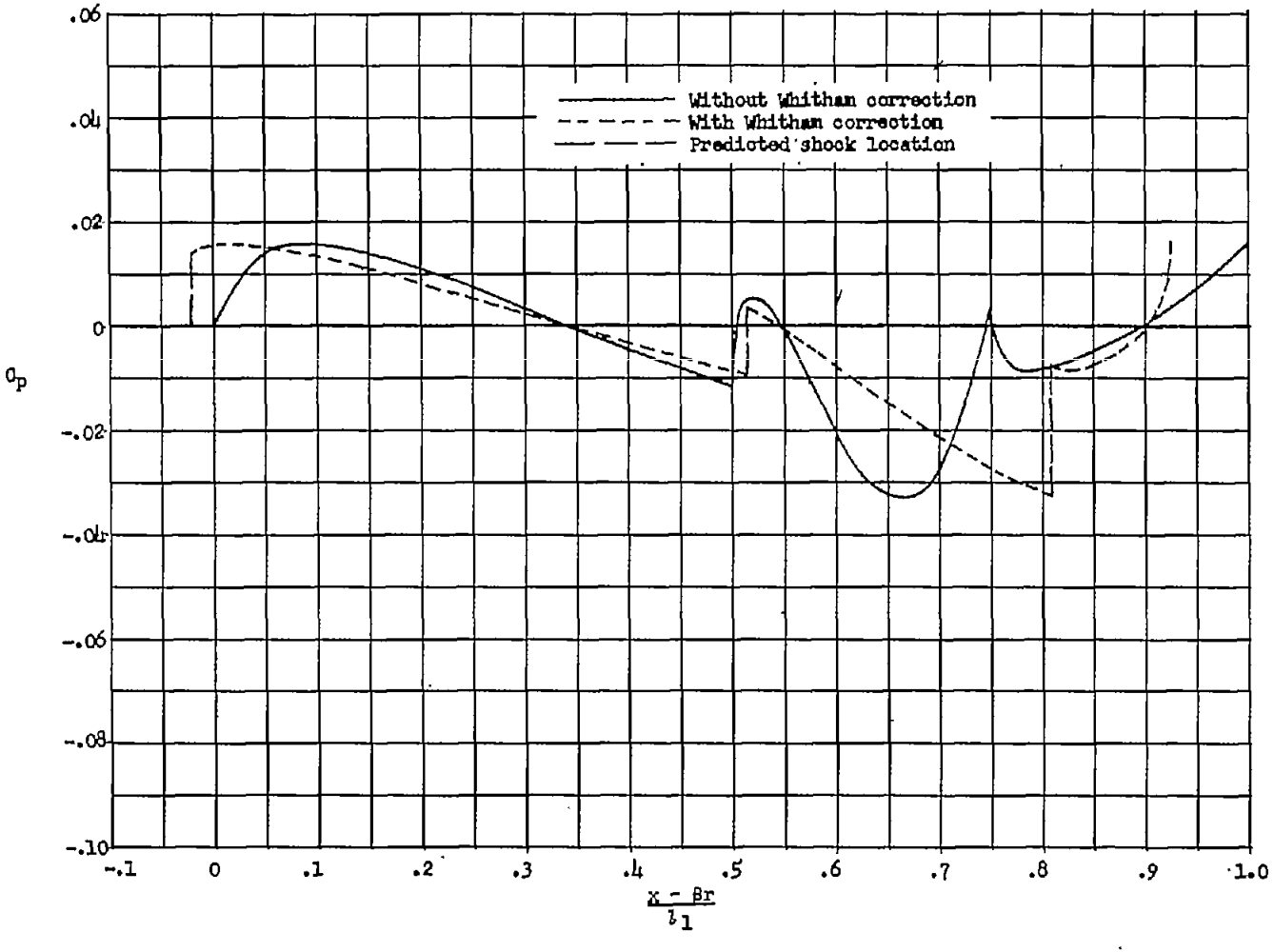

(d) $\frac{r}{l_1} = 1.0$.

Figure 10.- Concluded.

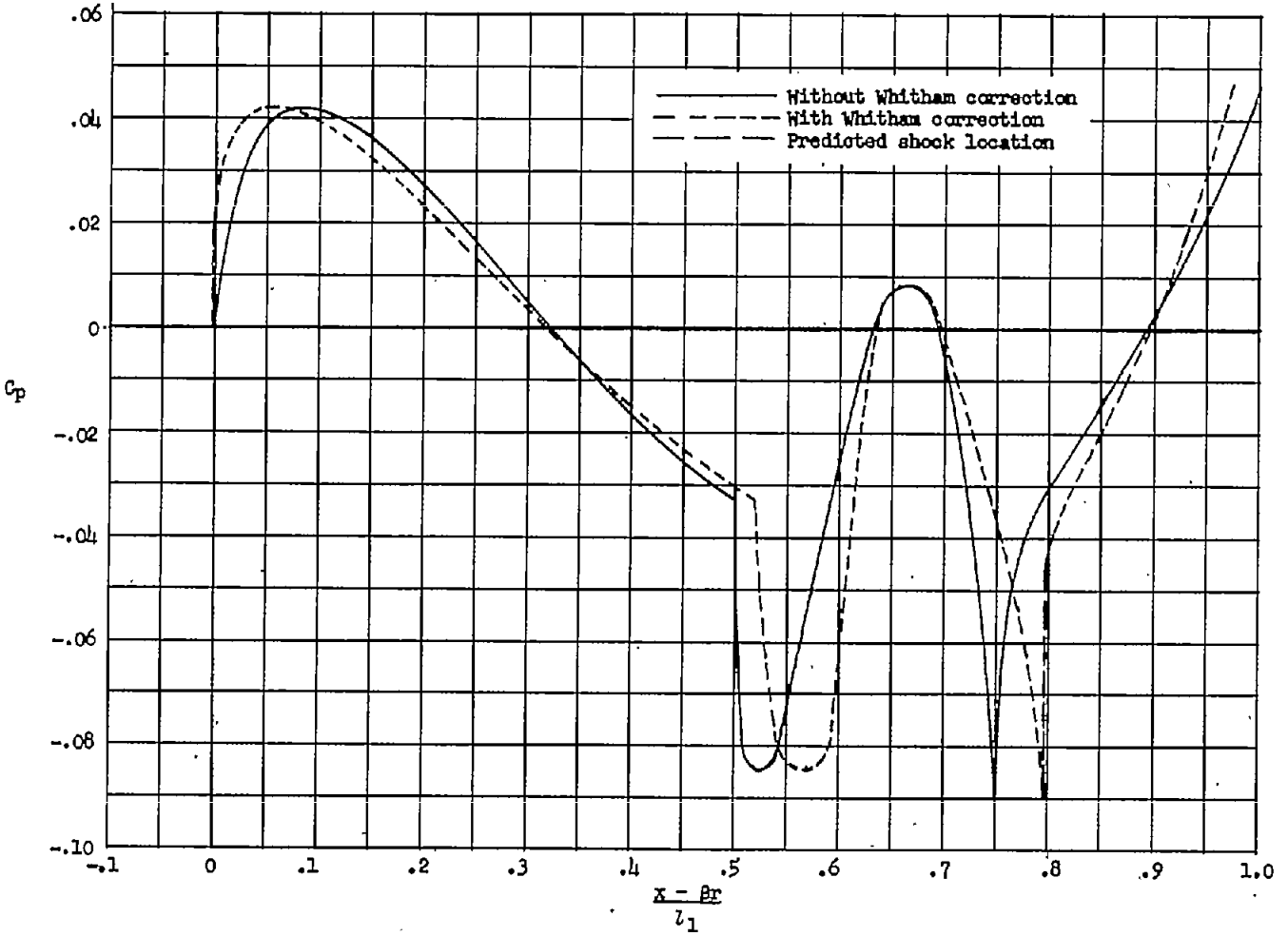

(a) $\frac{r}{l_1} = 0.125$.

Figure 11.- Linear field pressure distributions, with and without Whitham correction, for indented body of figure 4. $M = \sqrt{2}$.

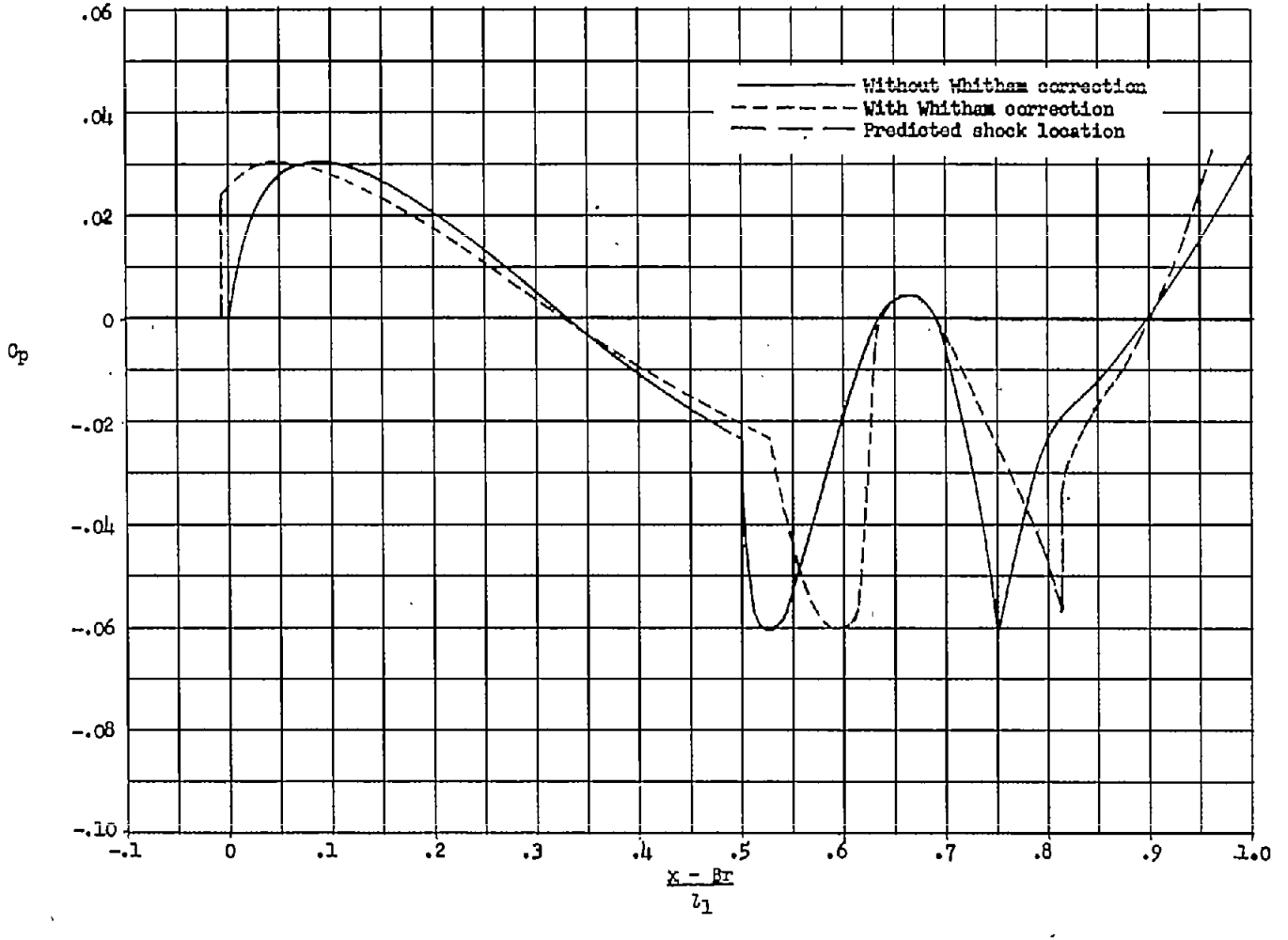

(b) $\frac{r}{l_1} = 0.250$.

Figure 11.- Continued.

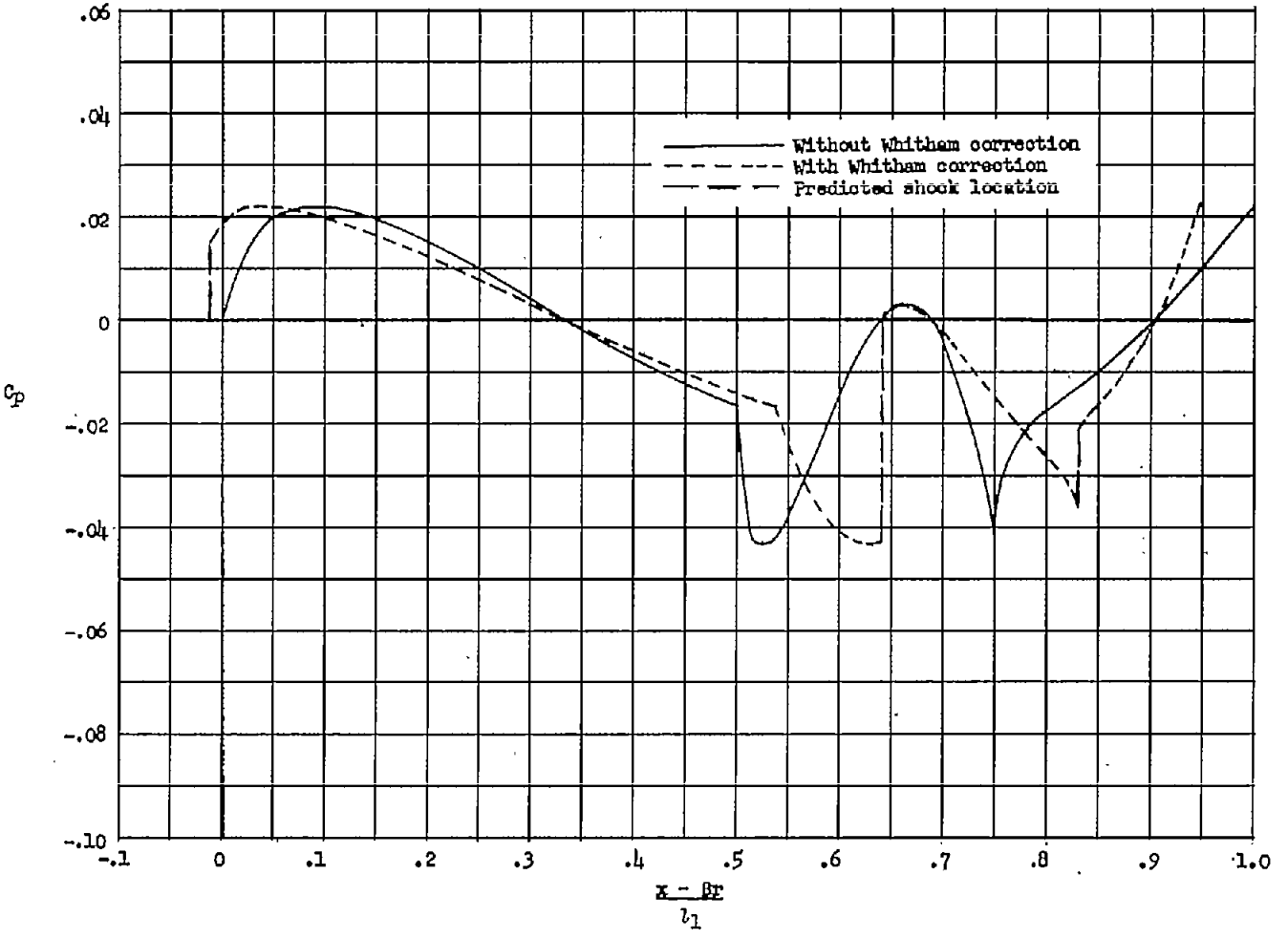

(c) $\frac{r}{l_1} = 0.500.$

Figure 11.- Continued.

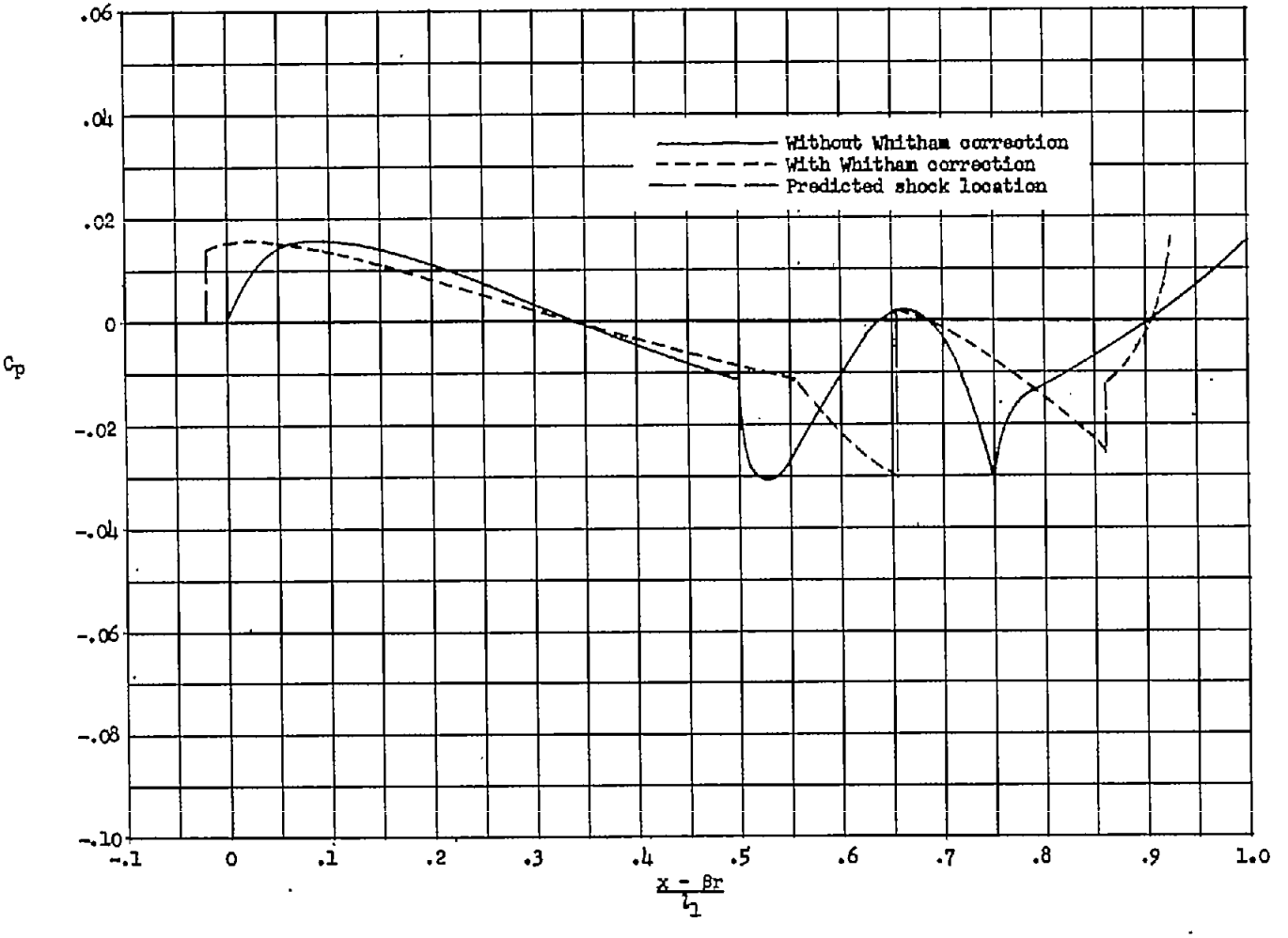

(d) $\frac{r}{l_1} = 1.0$.

Figure 11.- Concluded.

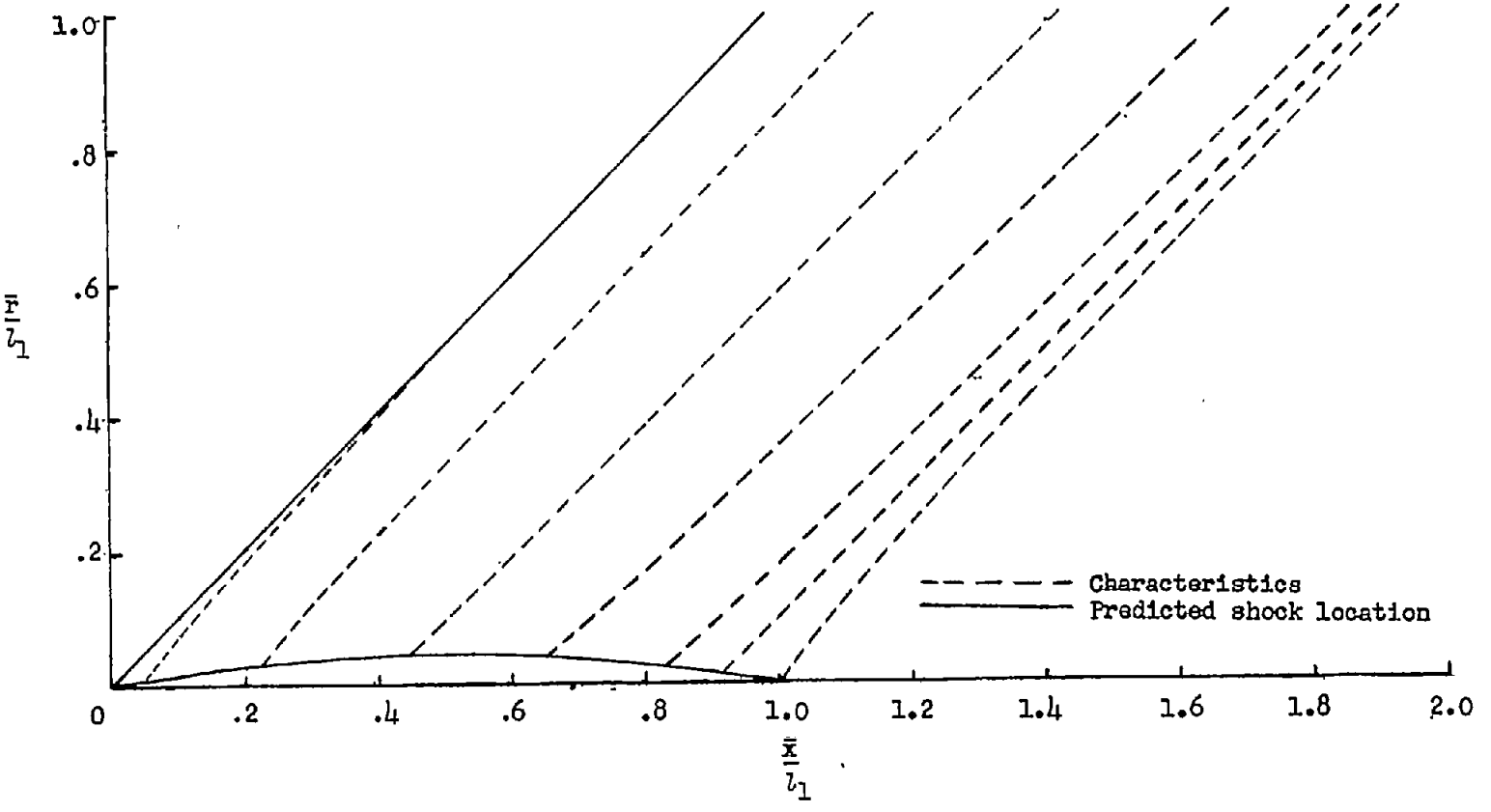

(a) Basic body.

Figure 12.- Characteristic field and shock locations predicted by Whitham theory for basic, bumped, and indented bodies of figure 4. $M = \sqrt{2}$.

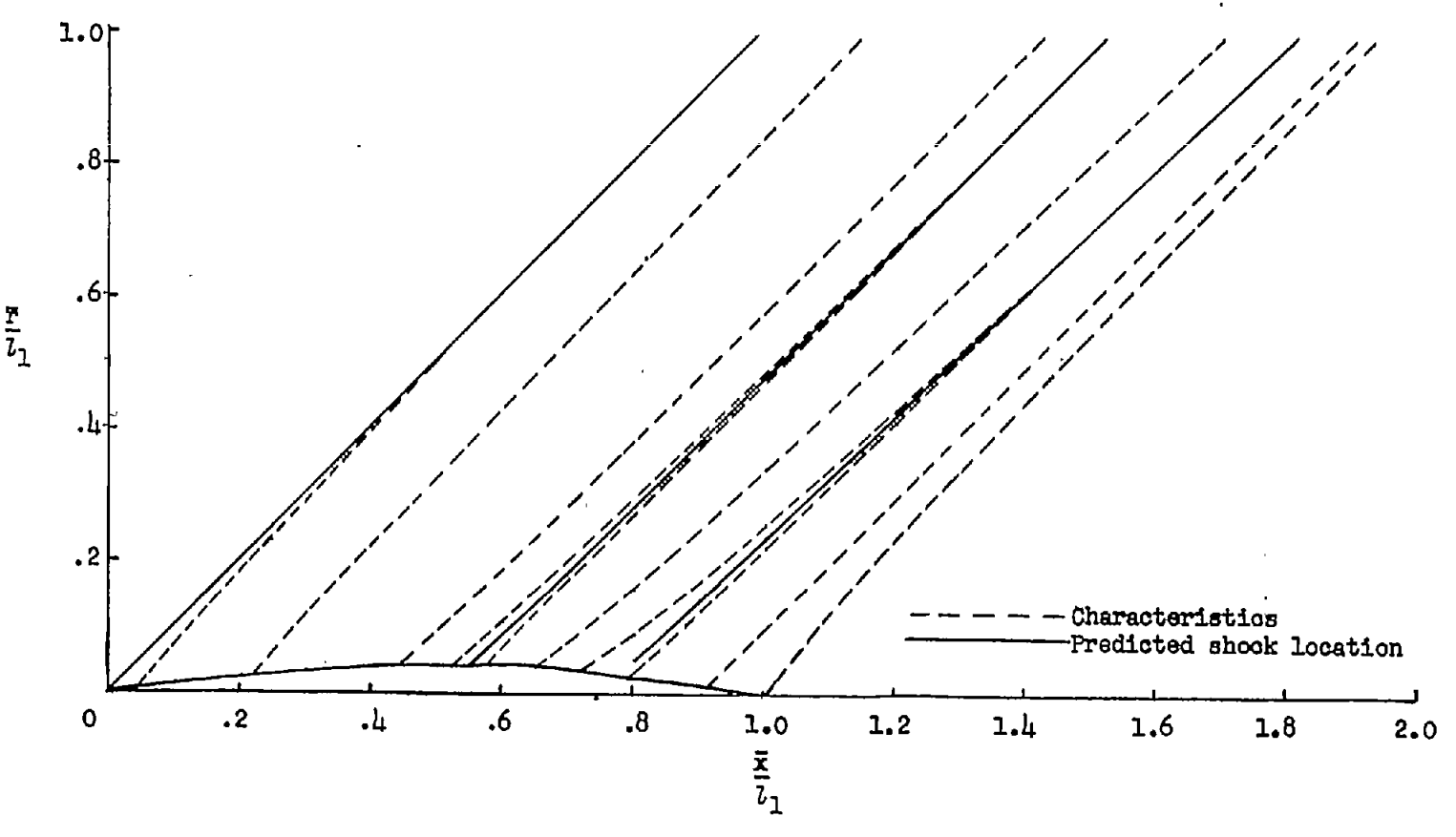

(b) Bumped body.

Figure 12.- Continued.

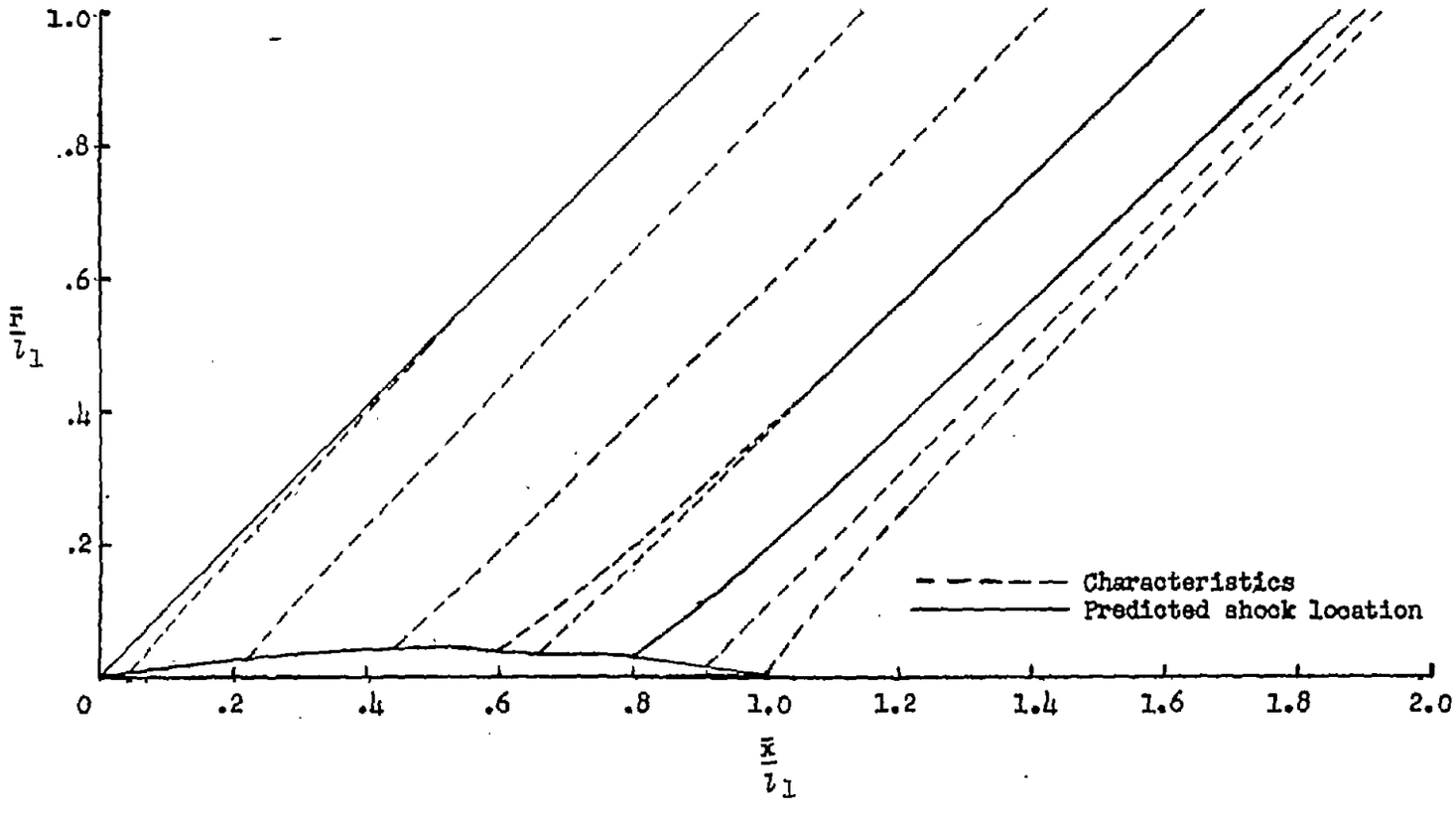

(c) Indented body.

Figure 12.- Concluded.

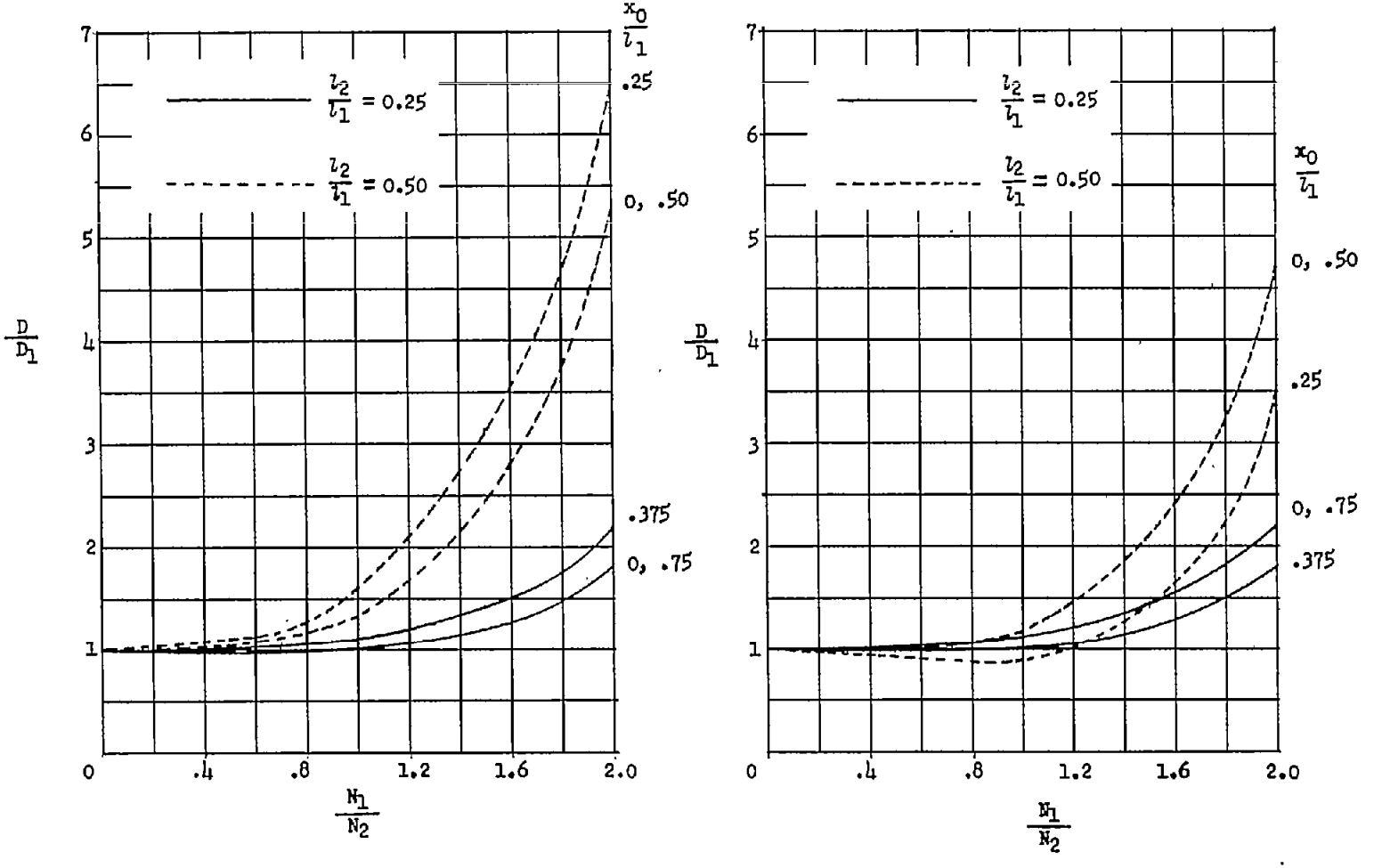

(a) Bumped body.

(b) Indented body.

Figure 13.- Variation of D/D_1 with N_1/N_2 for several values of length ratio l_2/l_1 and location x_0/l_1.

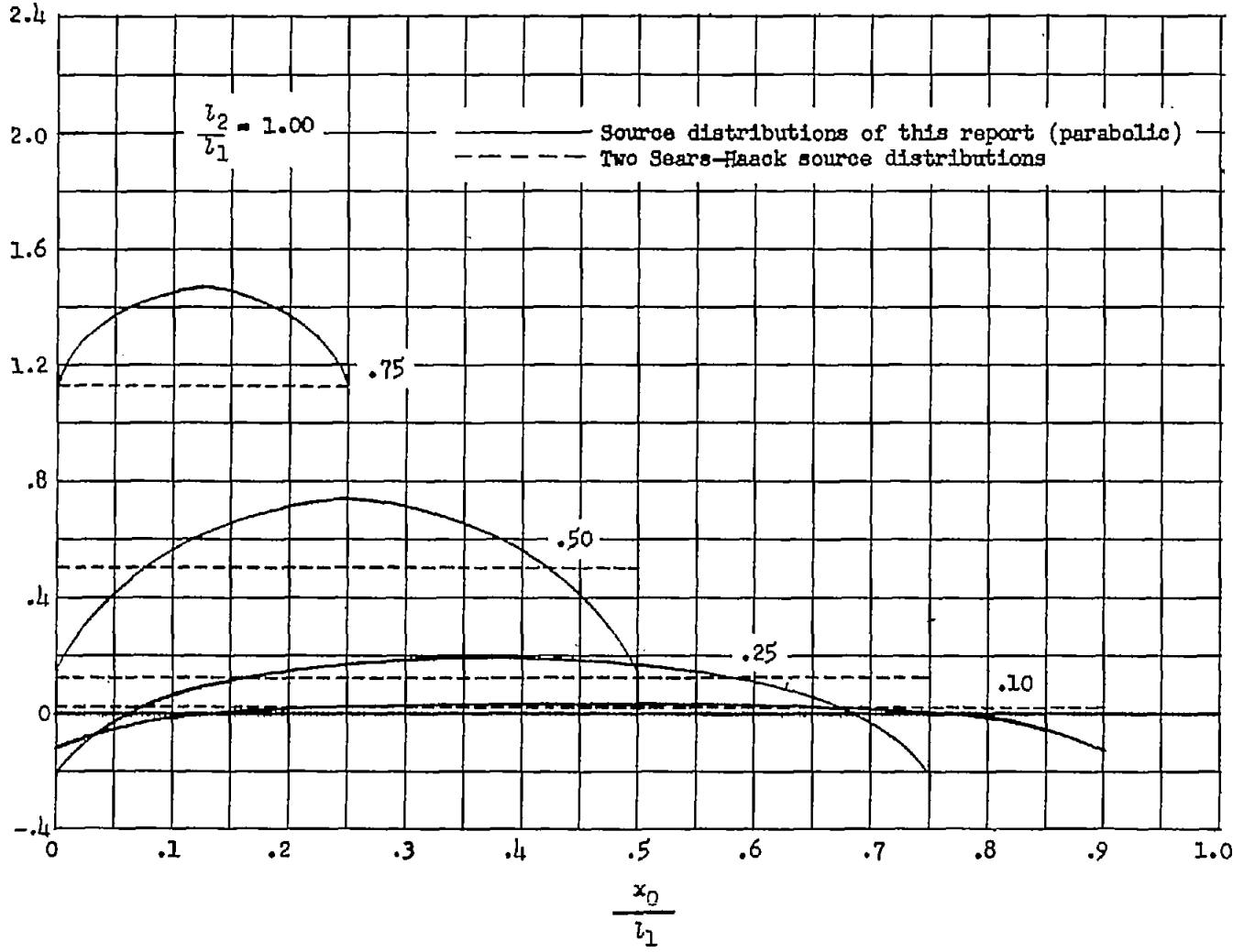

Figure 14.- Variation of the drag interference factor B with location x_0/l_1 and length ratio l_2/l_1.